A broadly applicable red dye doped Luminescent Solar Concentrator photo microreactor

Dobbelaar, J.

Award date:
2017

A broadly applicable red dye doped Luminescent Solar Concentrator photo microreactor

Jeroen Dobbelaar

Thesis submitted in partial fulfilment
of the requirements for the degree of

MASTER OF SCIENCE
in
CHEMICAL ENGINEERING & CHEMISTRY

Eindhoven, May 2017

Department of Chemical Engineering and Chemistry
Micro Flow Chemistry and Process Technology
Eindhoven University of Technology
Den Dolech 2, 5612 AZ Eindhoven, The Netherlands

Responsible Professor

Prof. dr. V. Hessel

Supervisor

Dr. T. Noël

Daily Supervisor

MSc D. Cambié

External Committee Member

Dr. M.G. Debije

Abstract

Due to rapid climate change, the need for greener chemistry is higher than ever. A way to achieve this greener chemistry is the use of visible light photoredox catalysis. Preferably, sunlight would be used to deliver the energy needed for these reactions. However, the use of sunlight in photochemistry is still very limited due to several challenges.

Previous research of our group[1] presented a cheap and straightforward reactor design which enabled photochemical reactions under solar light. This reactor was based on nature's way of harvesting light (e.g. tree leaf) and was able to increase the photon flux to the reaction channels by a four-fold compared to conventional reactors. The reactor was based on a combination of luminescent solar concentrators (LSCs) and flow photochemistry. LSCs are devices originally designed to generate electricity from sunlight when attached to a photovoltaic cell. However, in this research, LSCs are used to harvest sunlight and to deliver down-converted photons to microflow reaction channels, which replace the photovoltaic cell of the original LSC design.

Although promising results were obtained with these LSC photo microreactors (LSC-PMs), still some limitations are encountered due to the use of polydimethylsiloxane (PDMS) in the reactor design. Specifically, the direct contact between the PDMS and the reaction mixture causes some issues, such as swelling of the device and solvent induced leaching of the dye. In this work, a more stable device is created by adding solvent-resistant capillaries into the design of the device to prevent this direct contact. Several fluorinated capillaries have been tested to see the influence of the tubing dimensions and material to the optical performances of the device. The best results were obtained with the use of Tefzel tubing, while the dimensions of the capillary only influenced the light penetration depth. This result suggests that for this application, unlike conventional photo microreactors, the impact of the polymer refractive index is more significant than its transparency.

Despite the high photon efficiency, the PDMS based LSC-PM still encountered several drawbacks such as high costs, low rigidness and limited colour possibilities. To overcome these problems, polymethyl metacrylate (PMMA) has been investigated as matrix material. With this new reactor material, better performances could be obtained as one of the photon-loss mechanisms (i.e. escape cone losses) was mitigated by the higher polymer refractive index. Within the PMMA based LSC-PM, no significant influence of the different capillary materials was encountered. This research also presents several scaled up PMMA based LSC-PMs to perform hydroxylation reactions of arylboronic acids on a larger scale. These LSC-PMs significantly outperformed the conventional reactors. Lastly, different coloured LSCs have been investigated to widen to scope of the photochemical reactions towards more photocatalysts.

Table of Contents

1 Introduction

It has recently been stated by former president Barack Obama[2] that a change towards greener energy resources has to be made within a short period of time. Well-known effects of climate change such as rising sea levels and droughts are frequently observed, due to for example increasing carbon dioxide concentrations and depleting oil reserves. To be able to switch towards green energy, a change within the chemical industry is necessary. Possibilities which have been investigated intensely last decades are the use of flow chemistry[3] and photochemistry[4] to replace the harsh conditions of some traditional chemical reactions. Although, a lot of research has been focussed on these topics, the amount of flow photochemical reactions on industrial production scale are still limited[5].

Photochemical reactions have been studied for almost a century[6], however during recent years new interest was gained due to the introduction of visible-light photoredox catalysis[7]. Within this research it is aimed to create possibilities for the use of sunlight for visible-light photoredox chemistry. This has been achieved by combining luminescent solar concentrators with flow photochemistry mimicking the way tree leaves use sunlight within nature[8]. The use of sunlight for photochemical reactions offers both environmental and economic advantages, since the photons deliver a free, green and traceless[9] source of energy. Effort has been made to design a robust and easily scaled up reactor, to make the first small steps towards industrial applications.

2 Theory

2.1 Photochemistry in flow

Over the years, there has been an increasing interest in photochemistry[10]. Certainly visible-light photoredox catalysis has recently gained a lot of attention[11], since this could widen the scope of photochemical transformations and encourage the possibility of sunlight use. To perform photoredox catalysis, a photon is absorbed by a photocatalyst, resulting in electron or energy transfer reactions. These photons can be considered as green and traceless reagents[9], since these photons can be used in large excess without creating the need of an extra separation step. Therefore, photons can be used to accelerate the reaction kinetics without influencing the process mass intensity.

Traditionally, photochemistry was performed in batch reactors. However, performing photochemistry in microflow can deliver some huge benefits, such as better light irradiation, shorter reaction times and improved reaction selectivity[4]. Besides this, the large surface to volume ratio of a microreactor can create fast heat exchange and the large contacting surface within segmented flow can result in high mass transfer coefficients[12]. Some of these advantages will be discussed in more detail in this chapter.

2.1.1 Safety of operation

Due to the small dimensions and consequently small reactor volume of microreactors, the amount of chemicals that are present inside a microreactor is significantly lower than in a large batch vessel. The reduced amount of hazardous chemicals could decrease the risks and therefore increase the safety of operating chemical reactions.

2.1.2 Irradiation of the reaction mixture

To perform photochemical reactions, absorption of photons is needed (Grotthuss-Draper law). A homogenous energy distribution inside the reaction mixture is needed to achieve high selectivities and high yields[4]. The Beer-Lambert-Bouguer law states that the absorption of light travelling through a medium depends on the molar concentration (C) of the absorbing component, the length of the pathway (d) and the molar extinction coefficient (ε) as follows:

$$\mathrm{A} = \log_{10} \frac{I_0}{I} = Cd\varepsilon \qquad \textbf{(1)}$$

As can be seen from the Beer-Lambert-Bouguer law, the energy distribution over a reaction mixture is not homogeneous, due to absorption effects of the photocatalyst. Decreasing the dimensions (d) of the reactor could significantly decrease the differences in absorptions over the reaction mixture resulting in a more homogenous energy distribution. Figure 1 shows the relation between the reactor radius and the transmission through a reaction mixture containing a photocatalyst solution. It can clearly be seen that small reactor dimensions (microreactor technology) can result in a more homogenous energy distribution. Among other things, the better irradiation of the reaction mixture inside microreactors can significantly reduce the needed reaction time.

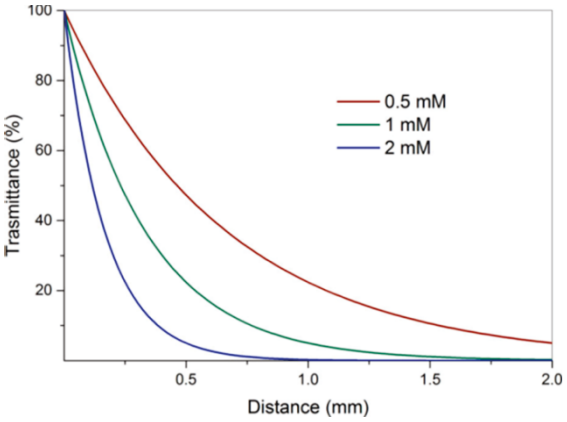

Figure 1: Transmission of light as function of the reactor radius in a photocatalytic reaction with $Ru(bpy)_3$ [ε= 13000 $cm^{-1} M^{-1}$]. (Picture obtained from [4])

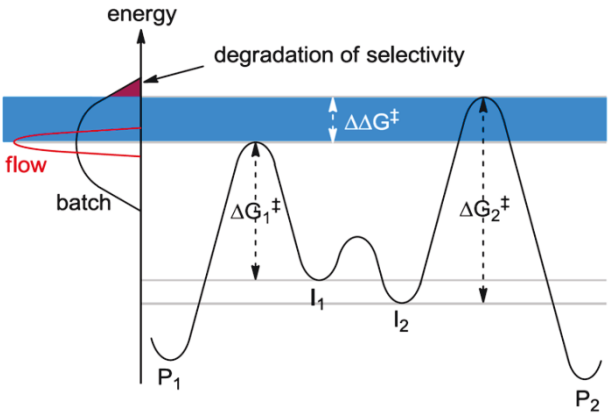

Figure 2: Energy diagram showing that the larger energy distributions within batch reactors compared to flow reactors can result in the formation of a side product (P_2) instead of the desired product (P_1)

2.1.3 Reaction selectivity

High selectivities are frequently aimed for a lot of chemical reactions. It is known that high selectivities can be achieved inside microreactors. This is most of the time a result of the large surface to volume ratio which creates perfect mass- and heat transfers[4]. The high heat transfer coefficients create a smaller energy distribution within microreactors compared to batch reactors, which can prevent the formation of some side products (see Figure 2). Also the described equal photon distribution can play an important role in achieving high selectivities. Besides the high surface to volume ratio, also the fact that the residence time inside a microreactor can precisely be tuned is beneficial. By variating the residence time inside the microreactor, the reaction can precisely be stopped before follow-up reactions (e.g. degradation) occur, enabling high selectivities. Lastly, the selectivity of photoredox reactions can be stirred by use of different light sources. A specific wavelength is needed for the activation of a photocatalyst. Other wavelengths could give rise to the formation of side products or could prevent the reaction to occur. A clear example of this can be found in the research of Itoh and co-workers[13]. Their research showed (see Figure 3) that variating the irradiation wavelength by using different filters in front of a Xenon lamp could tune the reaction yields of a cycloaddition reaction. When no filter was used, no product was obtained, since the substrates were probably decomposed by high-energy photons. The selectivity of this reaction can clearly be tuned by irradiating with the right wavelength.

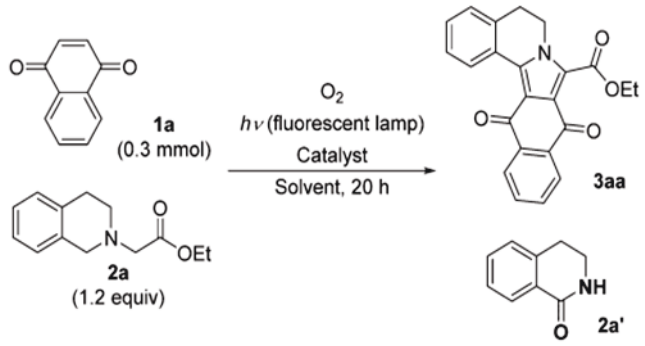

Wavelength irradiation	Yield
300 W Xe lamp (no filter)	0 %
300 W Xe lamp (405 nm)	14 %
300 W Xe lamp (610 nm)	17 %
300 W Xe lamp (660 nm)	54 %
No light	0 %

Figure 3: Yields of a cycloaddition reaction with the use of different filters in front of a 300 W Xe lamp. (Data obtained from [13])

2.2 Using sunlight for photochemistry

2.2.1 Chemistry

Ideally, sunlight would be used to deliver the photons needed for photochemical reactions, making the reactions green, sustainable and cost-efficient. There are however still some challenges facing the change towards sunlight driven photochemical reactions. Firstly, most of the sunlight in the Netherlands is diffused due to reflection and scattering by buildings or by trees[4]. This can decrease the performances of a photochemical reaction under sunlight. Large surfaces may therefore be needed to collect enough sunlight for the reactions. Furthermore, the light intensity can differ a lot over time, due to clouds and the day-night cycles. Therefore, light sensors might be needed to change the residence times of the reaction to ascertain full conversion at changing light intensities. Besides these effects, side reactions can easily occur due to the broad solar spectrum. As explained in chapter 2.1.3, the selectivity of a photochemical reaction can be stirred by irradiation at a specific wavelength. Since the solar spectrum is very broad, a mismatch between the emission spectrum of sunlight and the absorption spectrum of the photocatalyst is present. This enlarges the change of undesired side reactions and the formation of by-products.

Due to these difficulties, the amount of photochemical reactions using sunlight is limited on both industrial- and lab scale. On the industrial scale, most sunlight driven photochemical reactions are performed on the disinfection of water[14]. Besides this, reactors such as the PROPHIS reactor (see Figure 4A[15]) or SOLFIN reactor (see Figure 4B[16]) have for example been designed for other photochemical reactions. Although these reactors performed well, they were quite expensive due to the largely sized moving panels. Furthermore, these reactors were only able to handle direct light irradiation, whereas the large fraction of diffused light is not efficiently being used[17].

In a recent lab scale research[18], a reactor for sunlight driven photochemical reactions was designed. To create an area which was able to collect enough sunlight for the reaction, 25 meter of tubing was needed (see Figure 4C). This large amount of used capillary resulted in a significant pressure drop over the reactor. Furthermore, side reactions could occur in all these reactors due to the irradiation of the broad solar spectrum.

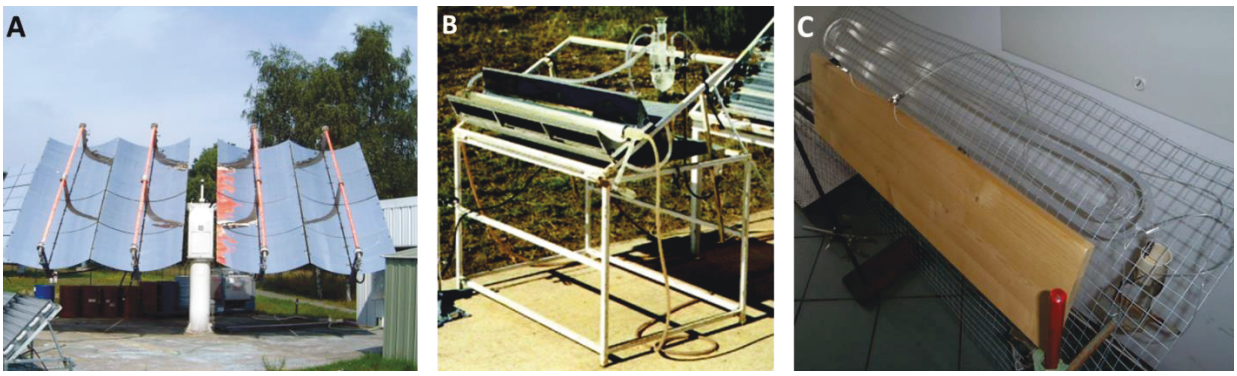

Figure 4: Examples of macro (A), meso (B) and micro (C) scaled sunlight driven photochemical reactors (Pictures obtained from [15](A), [16](B) and [18](C))

2.2.2 Nature

In contrast to chemistry, which is still facing some challenges in performing photochemistry with the use of sunlight, nature has already been able to perform these reactions for a long period of time. For example, tree leaves are able to convert sunlight energy into chemical bonds in a flexible and lightweight "reactor" (the leaf itself). It is important to firstly understand nature's way of using sunlight, before we are able to mimic this for the use of sunlight in photochemistry.

To understand nature's way of using sunlight, the light harvesting mechanism of a tree leaf is investigated in more detail. Within a tree leaf, several reaction centres are present. Inside these reaction centres photosynthesis is performed by producing energy rich products (e.g. ATP) via photo-induced reactions[8]. These energy rich products are later on used to convert CO_2 into carbohydrates and other cell consituents[19].

Around these reaction centres, many chromophores which are bound in light-harvesting complexes are present. After absorption of a solar photon by a chromophore, the chromophore enters an electronic excited state. Via several light-harvesting proteins (chromophores) this excitation energy is funnelled towards a reaction centre[19]. Due to the many absorbing and transporting proteins, large amounts of energy are transported to the reaction centres enabling multiple photochemical reactions in a fraction of a second. Most photosynthesis reactions inside a reaction centre require however multiple turnovers and therefore multiple electron transfer events are needed at the same time inside a reaction centre. These simultaneous electron transfer events can be achieved due to the many surrounding chromophores. Figure 5 shows a schematic overview of the electron transfer events inside a tree leaf. Besides tree leaves, also some bacteria are known to be able to harvest light towards reaction centre. An extreme example are the light harvesting properties of the bacteriochlorophyll-e, which is found in the Black Sea at depths of 80 metres[20]. Due to its good light harvesting properties, the bacteria can survive at conditions with extremely low light irradiation.

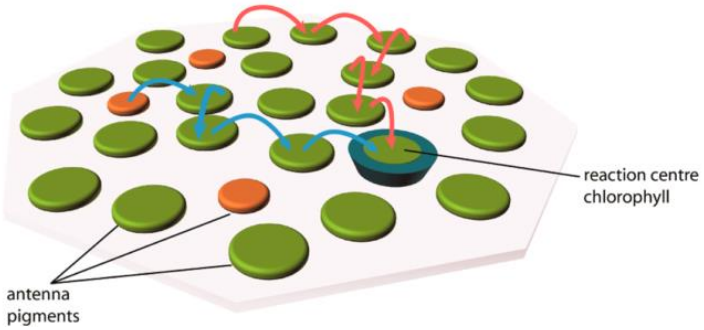

Figure 5: Schematic overview of electron transfer events inside a tree leaf. (Picture obtained from [19])

2.3 Luminescent Solar Concentrator

Within this research, luminescent solar concentrators (LSCs) will be used to produce photochemical reactors. LSCs consist of luminescent dyes dispersed into a transparent glass or polymeric waveguide. These luminophores are able to absorb incoming sunlight. Also incoming diffused sunlight can be absorbed by the luminescent dyes. After absorption, the light is re-emitted by the luminophores. A fraction of this re-emitted light is guided towards the edges of the LSC. Photovoltaic cells, which are attached to the edges of the LSC, are able to convert this guided light into electricity[21] (see Figure 6). LSCs are less expensive than photovoltaic cells. LSCs can therefore increase the efficiency of an expensive solar cell by enlarging the sunlight collecting surface[22]. Due to high oil prices (during the 1980s) and climate change awareness (nowadays), a lot of research has been carried out on LSCs[21].

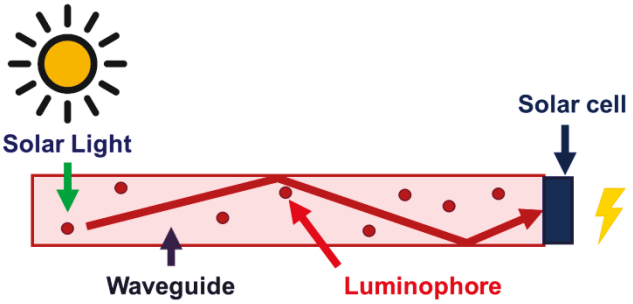

Figure 6: Schematic overview of a luminescent solar concentrator. Incoming sunlight is absorbed and re-emitted by a luminophore. A fraction of this light is guided towards an attached solar cell at the edge of the LSC.

Different fluorescent dyes can be dispersed inside a LSC resulting in different coloured LSCs. After absorption of a photon of the incoming light by a fluorescent dye, the dye reaches an excited state. This exited state will firstly undergo some non-radiative relaxation steps (e.g. vibrations) before the photophysical decay of the excited state results in the emission of another photon (i.e. fluorescence) (see Figure 7, left). According to the law of conservation of energy, the energy of the re-emitted photon has to be lower than the energy of the absorbed photon. Therefore, the peak of the re-emitted light is at a longer wavelength than the absorbed light (Stokes shift). This effect is called down-conversion and is clearly visible in Figure 7. It can be seen that a dispersed red dye (BASF Lumogen Red 305) re-emits the light at longer wavelengths compared to the absorption of the light by this dye. To conclude, a LSC is able to focus and down-converted both direct and diffused light.

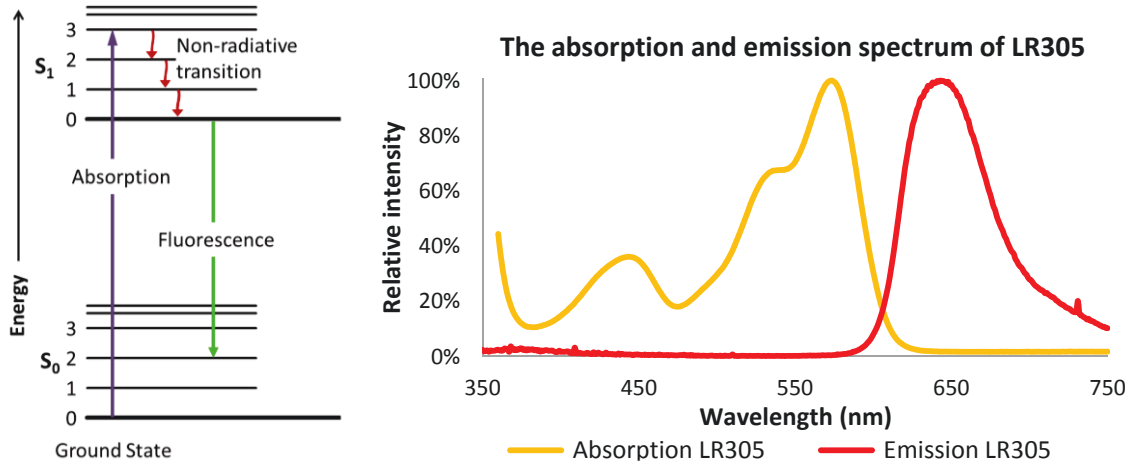

Figure 7: Left: An example of a Jablonksi diagram showing the concept of absorption and fluorescence, Right: The absorption and emission spectrum of a red dye (LR305) doped PMMA based LSC plate

2.3.1 Light transport

Since the fluorescent dye is embedded inside a high refractive index material, the re-emitted photons are trapped inside this material and eventually guided through the LSC towards the edges of the plate. This effect will be explained in more detail.

Snell's law describes the angles of light moving from one medium to another medium. This law states that the refraction angle (θ_2) is only dependent on the angle in the incoming light beam (θ_1) and the refractive indexes of the two media (n_1, n_2)(see Figure 8), following the equation:

$$\frac{n_1}{n_2} = \frac{\sin\theta_2}{\sin\theta_1} \quad \textbf{(2)}$$

The guided light can reach the LSC-air interface at different angles, among which also large angles are present. When travelling from high to low refractive index media (e.g. from a LSC towards air), total internal reflection will occur when light reaches the interface above a critical angle (θ_c). In that case, all the light is reflected and stays inside the LSC device. Therefore, the light can be guided towards the edges of the device. This critical angle (θ_c) can be calculated by use of the following formula:

$$\theta_c = \sin^{-1}\frac{n_2}{n_1} \quad \textbf{(3)}$$

Since the refractive index of air (n_2) stays constant, the critical angle could be lowered by using higher refractive index LSC materials (n_1). Smaller critical angles enlarge the change of total internal reflection and could therefore increase the amount of light transported to the edges of the LSC.

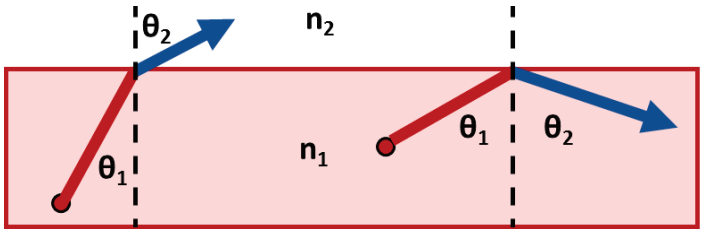

Figure 8: Schematic overview of refraction of light (left) and total internal reflection (right) when moving from a high RI medium (1, LSC) to a lower RI medium (2, air)

2.3.2 Light losses

Unfortunately, LSCs still achieve up to moderate efficiencies. The highest reported efficiencies of LSCs in combination with photovoltaic cells are around 7.1%[23]. These low efficiencies are mostly caused by the losses which appear in the LSC design and in the photovoltaic cell. A few of the loss mechanisms[21] within the LSC design will be discussed in more detail.

The direction of the re-emitted light from a fluorescent dye is perpendicular to the absorption dipole of the dye molecule (see Appendix IV). It can be assumed that within this research the dye molecules inside the used LSCs are mostly randomly orientated. The re-emitted light can therefore be considered as approximately isotropic over the complete LSC. For this reason, re-emitted light can also reach the air-LSC interface at smaller angles than the critical angle (i.e. within the escape cone) (see chapter 2.3.1). In that case, the re-emitted photon will not be guided through the matrix, but escape from the LSC (Figure 9, 1). Research has been performed to align fluorescent dyes with help of liquid crystals to direct the re-emission and consequently minimize the amount of light losses via the escape cone[21].

Another loss mechanism which can be encountered inside LSCs are re-absorption losses. These losses can be caused due to a possible overlap between the emission and absorption spectrum of a dispersed fluorescent dye. When this is the case, a re-emitted photon could be re-absorbed by another dye molecule instead of being guided towards the edges of the device (Figure 9, 2).

Furthermore, some of the absorbed photons will not be re-emitted as lower energy photons by the dye molecules due to non-unity emission quantum yield. Instead this energy will be lost as vibrations or heat (Figure 9, 3c).

Besides this, light could pass through the LSC device without being absorbed by a luminophore (Figure 9, 3a). This is mostly caused by the limited absorption bands of the dispersed luminophores. Also imperfections in the waveguide surface (Figure 9, 5d) or within the waveguide matrix (Figure 9, 5c) can result in losses due to scattering. Lastly, entering light could partly be reflected at the top of the LSC (Figure 9, 5a). This would lower the amount of light which can reach the dye molecules.

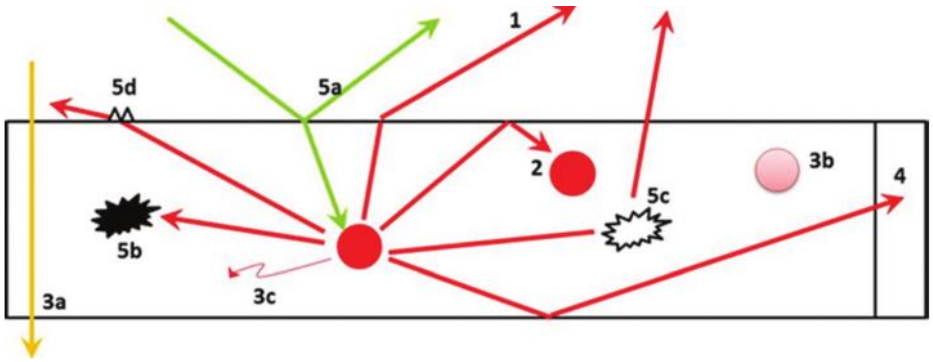

Figure 9: Overview of different possible losses inside a LSC (Picture obtained from [21])

2.4 Combining LSC and Photochemistry

2.4.1 Theoretical

To be able to mimic nature's way of collecting sunlight within a tree leaf, LSCs and flow photochemistry were combined. Instead of attaching a photovoltaic cell to the edge of a LSC (see Figure 6), micro reaction channels were placed inside the LSC plates (see Figure 10) creating a luminescent solar concentrator photo microreactor (LSC-PM). This design offered several advantages.

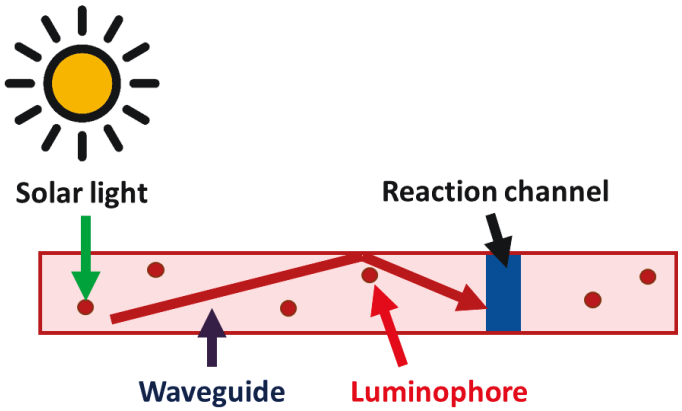

Figure 10: Schematic overview of a LSC-PM, where a reaction channel is placed inside a LSC

First of all, due to the ability of LSCs to concentrate light, an increased amount of light can reach the reaction channels. This includes both direct and diffused light. This effect is particularly appealing for sunlight use, since the limited amount of direct sunlight irradiation in the Netherlands requires large reactors (see chapter 2.2.1). In analogy to the reaction centres of a tree leaf, which collects photons from several chromophores (see chapter 2.2.2), the reaction channels inside the LSC-PM design receive photons from several surrounding dye molecules.

Secondly, the down-conversion effect of LSCs can play an important role. As explained, side reactions can occur when performing photochemistry under solar light due to the broad solar spectrum. As can be seen in Graph 1, the photocatalyst (Methylene blue, Graph 1, blue line) most strongly absorbs a fraction of the solar spectrum (Graph 1, grey line) in the range of 550 till 700 nm. The weakly and non-absorbed part of the solar spectrum could give rise to side reactions and is not efficiently used. Within a LSC-PM, this part of the solar spectrum is absorbed by the dispersed luminescent red dye (LR305, Graph 1, red line). After absorption, the dye re-emits the light (Graph 1, green line) in a range of wavelengths that matches the absorption peak of the photocatalyst. This re-emitted light can therefore efficiently be used by the photocatalyst to accelerate the photochemical reaction. This down-conversion effect could therefore decrease the amount of side reactions and result in an efficient use of light which would otherwise be lost.

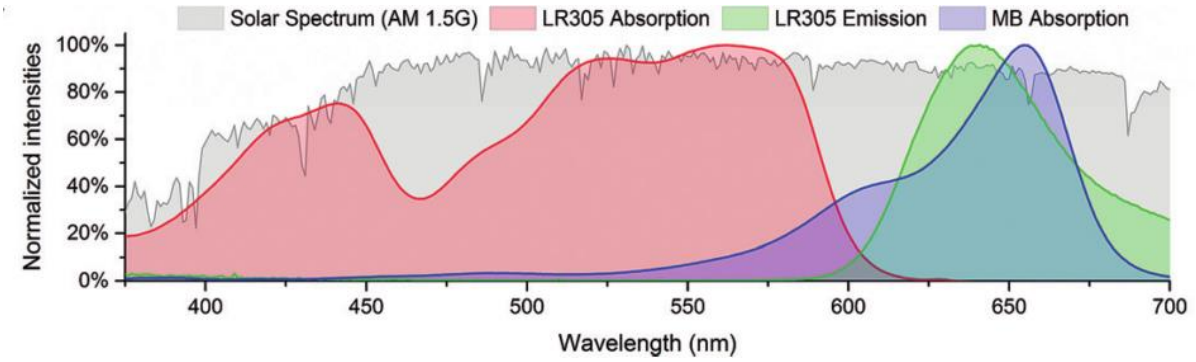

Graph 1: Emission and absorption spectrum of the luminescent red dye (LR305) inside a PDMS based LSC and absorption spectrum of the photocatalyst (MB) in acetonitrile. A good overlap between the emission spectrum of the dye (green) and the absorption spectrum of the photocatalyst (blue) can be seen. (Picture obtained from [1])

Besides Methylene blue, other photocatalysts could be needed for different photochemical reactions. These different photocatalyst each have an absorption peak at other wavelengths. To be able to use the LSC-PM design with different photocatalysts, the emission peak of the dispersed luminophores should shift to the same range as the absorption peak of the photocatalyst. Changing of the absorption and emission peak of the LSC-PM can be achieved by dispersing a different coloured fluorescent dye inside the reactor. Therefore, different coloured reactors could create possibilities for the use of different photocatalysts, widening the scope for photochemical reactions.

These positive effects could result in a highly efficient flow reactor for performing photochemistry under sunlight. Besides this, the used design is simple and non-expensive.

2.4.2 Experimental prove of concept

Recently, a paper of our group was published[1], introducing the LSC-PM concept. A red dye (LR305) doped PDMS based LSC-PM was designed and tested under both indoor and outdoor conditions. Blue LEDs were used to test the down-conversion effect (see Figure 11A). The emission of the blue LED light has a complete mismatch with the absorption of the methylene blue photocatalyst. Due to the down-conversion effect by the LSC-PM the reaction however still occurred. It was proven that higher doping (up to 200 ppm) of the luminescent dye (LR305) increased the performances of the reactor (see Figure 11A).

To test the light harvesting effect of the LSC-PM, the reaction channel was covered for direct irradiation. Only light which was guided through the LSC could reach the reaction channel to perform the reaction. This set-up was tested under a solar simulator. Also here it was found that higher dye doping increased the performances (see Figure 11B), proving the light harvesting character of the LSC-PM. Performing a reaction under a solar simulator with the use of a LSC-PM, showed a clear acceleration of the reaction when using higher doping concentrations of the dye (Figure 11C). The reaction was accelerated more than four-fold compared to the non-doped device.

After indoor tests, the 200 ppm doped reactor was also tested outdoor on a partly sunny day. The significant better performances of the doped LSC-PM compared to the non-doped reactor were also clear during these tests. It was also found that clouds, which create diffused light, had a significant smaller impact on the doped LSC-PM. This proves the fact that the designed LSC-PM can also handle diffused light quite well and is not limited to direct irradiation.

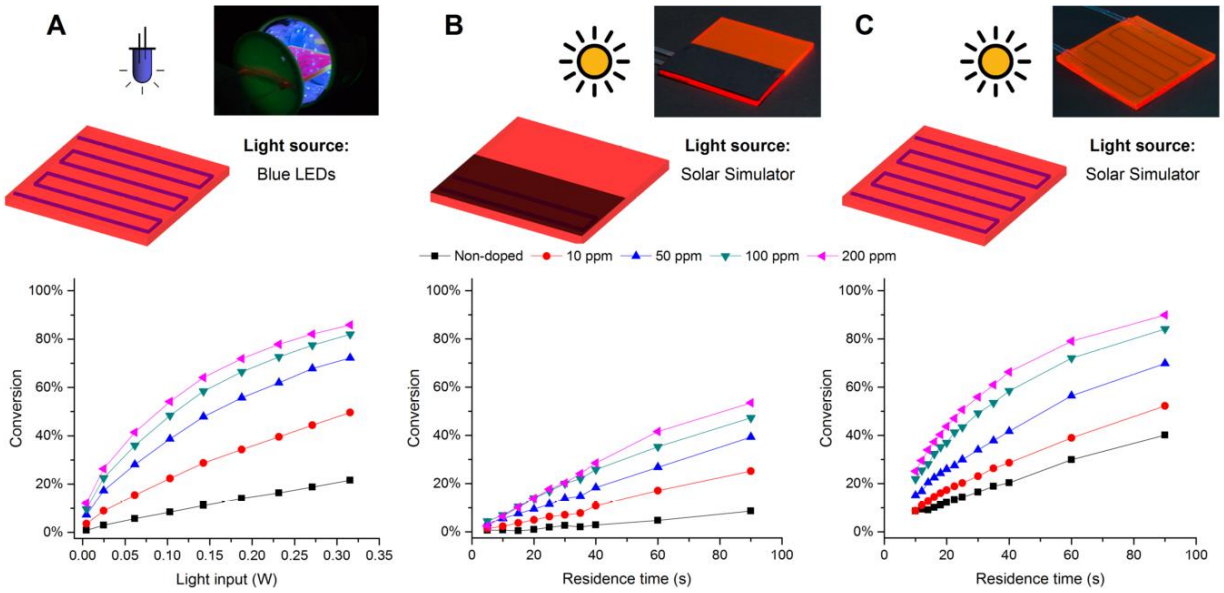

Figure 11: LSC-PMs tested at different dye-loadings. A) Test under blue LED irradiation proving the down-conversion effect, B) Test with partial coverage proving the light harvesting properties, C) Test under solar simulator. (Picture obtained from [1])

3 Problem Statement

Although promising results were obtained using PDMS based LSC-PMs (see chapter 2.4.2), still some limitations were present. In this chapter, different issues, which occur when using the PDMS based reactors, are explained.

3.1 Matrix swelling

One of the most striking limitations of the PDMS based LSC-PM is the limited compatibility of the reactor with different reaction solvents. It is known that PDMS can significantly swell when getting in contact with a number of organic solvents[24]. These solvents tend to diffuse into the PDMS, causing the swelling. It has been shown that mostly nonpolar or slightly polar solvents are incompatible with PDMS. Graph 2 shows the relative swelling of different organic solvents compared to their refractive index. Only the solvents within the grey box can be used in the current design of the LSC-PM without causing any significant swelling. Due to the direct contact between the reaction solvents and the PDMS based reactor, the solvents within the white area will swell the PDMS and destroy the LSC-PM (see Figure 12A).

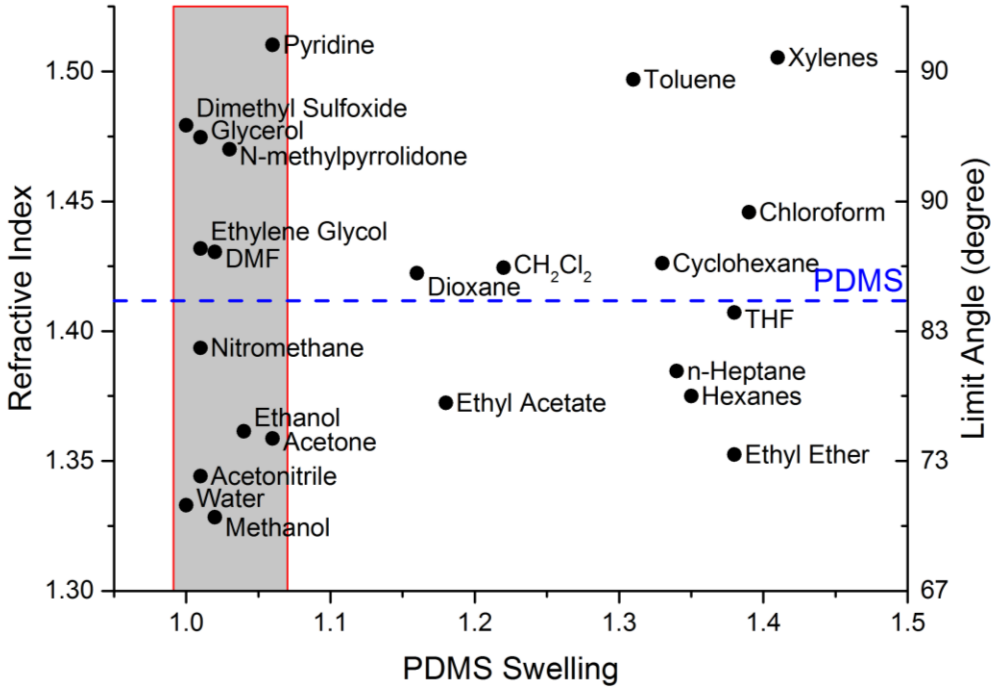

Graph 2: Relative swelling of PDMS when getting in contact with different organic solvents compared to the refractive index of these solvents. (Data obtained from [24])

3.2 Luminophore compatibility

As been explained in chapter 2.4.1, the use of different coloured LSC-PMs could create possibilities for reactions with different photocatalysts. Therefore an attempt was made to disperse different luminophores into the PDMS matrix. However, due to the polar character of for example the K160 dye, crystals were formed in the apolar PDMS matrix at already low doping concentrations (see Appendix IV for molecular structure). This made it difficult to manufacture devices with the needed optical density in other colours than the used red dye (LR305). The restriction to the red coloured LSC-PM, limits the amount of possible photochemical reactions significantly.

3.3 Leakage

The in- and outlet connections of the reactors are created by insertion of tubing by press and fit into the flexible PDMS based LSC-PMs. Since these connections are really loose, rapid leakage of the reactor due to any (back) pressure on these fittings frequently occurs. Besides this, the small dimensions of the plates and the flexible character of PDMS, make the reactor very fragile. Therefore, the reactors need to be handled very carefully.

3.4 Dye stability

Once a successful LSC-PM is manufactured, it is meant to operate for a significant amount of time outdoor under solar conditions. To investigate the long-term stability of the PDMS based LSC-PM, the absorbance of some red dye doped devices was measured over time, while being exposed to simulated solar irradiation (Atlas SUNTEST XXL, wavelength 300 – 400 nm). Graph 3 shows the rapid decrease in absorption of the devices with different dye loading. After 18 months of solar irradiation, the absorbance of the 200 ppm LSC-PM decreased with 56%. This would result in a significant decrease in the performances of the LSC-PM within a relatively short period of time. To conclude, the designed LSC-PMs could only perform well during a limited period of time.

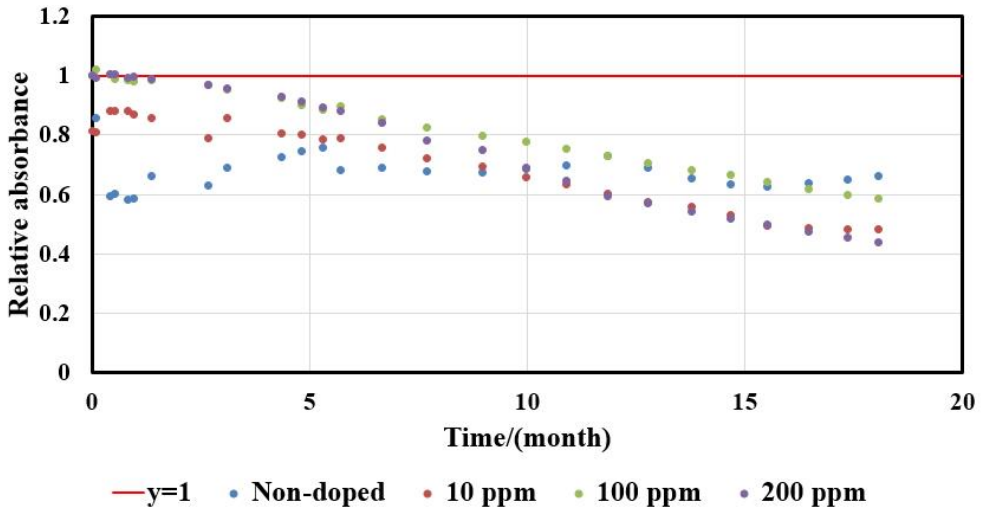

Graph 3: The relative absorbance of different dye (LR305) doped PDMS plates after being exposed to simulated solar irradiation (300-400 nm, 65 W/m^2, 40 days). (Data obtained by F. Zhao)

3.5 Slug flow merging

It is known that segmented (Taylor) flow can significantly enlarge the gas-liquid contacting areas and consequently improve mass transfer coefficients[12]. For this reason, segmented flow is frequently used in micro flow technology. Attempts to perform segmented flow inside the LSC-PM did however not result in a stable slug flow. The created slugs mainly merged when flowing from the fitted inlet tubing into the reactor. Besides that, the very high gas permeability of PDMS[25] might reduce the gas fraction of the segmented flow over time when using long residence times.

3.6 Dye leaching

The direct contact between the dye doped reactor and the reaction mixture, can cause leaching of the dye from the PDMS matrix to the reaction solvent flowing in the reaction channel. It was shown that flushing the reactor with toluene can result in a red coloured reaction mixture leaving the reactor (Figure 12B) and in removal of the red dye from the reaction channels in the PDMS matrix (Figure 12C). UV-VIS measurements proved that the red colour was indeed the red dye leaching from the reactor (see Appendix I, Graph 15). The leaching of the dye would destroy the reactor and consequently result in lower reactor performances. Additionally, the complete solar spectrum will be able to reach the reaction mixture in the leached reactor, enlarging the chance of side reactions. Last but not least, the contamination of the reaction mixture with the red dye results in the need of an extra unexpected separation step during the cleaning up.

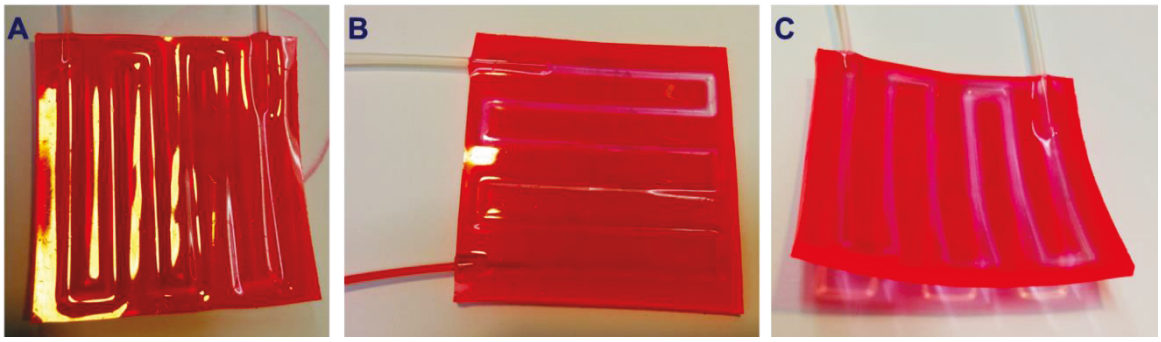

Figure 12: A swollen LSC-PM (A), Leaching of the dye from the PDMS matrix while flushing with toluene (B) results in a reactor where most of the dye proximity to the reaction channels is leached from the device (C).

3.7 Project aims

In this report, an effort has been made to overcome the previous described issues. The aim is to create a broadly applicable, chemical resistant and stable LSC-PM. The first step to achieve this, is preventing the direct contact between the PDMS based reactor and the reaction mixture, since this causes most of the limitations. To overcome this direct contact, capillaries will be added into the reactor design. Once this is achieved, the LSC-PM will be optimized. Furthermore, a different reactor material will be tested to overcome the fragile character of the reactor, the limited dye stability and the limited luminophore compatibility.

While creating a chemical resistant and stable LSC-PM, also new manufacturing methods for the reactor will be investigated, since the current approach is quite specific and difficult to scale up towards industrial applications. The scale up potential will also experimentally be tested.

Till now, only test reactions at very low substrate concentrations are performed inside the LSC-PM[1]. In this study, an attempt will therefore be made to perform a photochemical reaction in a scaled up device to show the possibility to produce chemicals within the LSC-PM.

4 Polydimethylsiloxane (PDMS)

In this chapter, the addition of capillaries into the PDMS based LSC-PM is investigated. Once capillaries are added into the design, the effect of different tubing materials and inner diameters is studied. Finally, the newly designed reactor will be compared with the previous reactor design without capillary and an attempt to scale up the capillary based PDMS design will be made.

4.1 Production method

4.1.1 Production method without capillary

To be able to explore a new manufacturing method for the LSC-PM, it is important to understand how to produce a PDMS based LSC-PM. This method has been extensively described by Cambié et al[1]. In this chapter, this method will be described both in general (see Figure 13) as well as in more detail (see Figure 14) before explaining new options.

To create the reactor, both a 3D-printed positive relief mould and a petri dish are filled with PDMS. After thermally curing, the 2 mm thick PDMS layer from the mould will be bounded to the 1 mm thick PDMS layer from the petri dish with the use of plasma oxygen resulting in the desired LSC-PM. This production process creates a lot of freedom in the design, since the 3D-printed moulds can be printed in almost every desired shape.

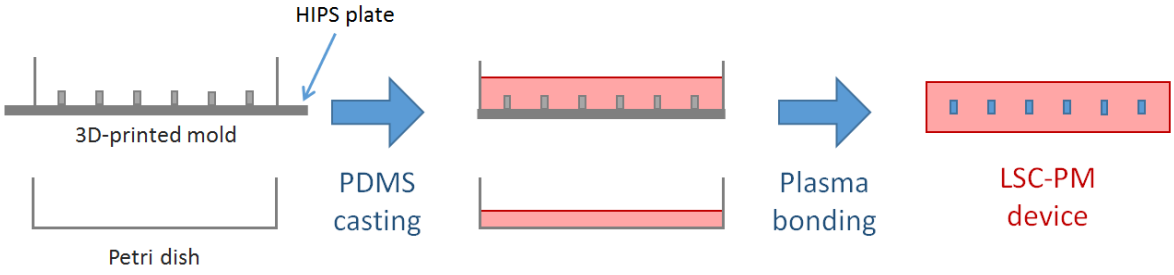

Figure 13: Schematic overview of the production process of the PDMS based LSC-PM without capillaries

Figure 14 shows the production process in more detail. Firstly, PDMS base and curing agent (Sylgard 184) are mixed together with a spatula in a 10:1 ratio (A+B). A solution of the red dye (Lumogen F Red 305) in diethyl ether is added to the PDMS mixture (C+D). The dye doping concentration could be calculated by using the following formula:

$$Y\ ppm = X\ g\ PDMS + \frac{X}{10} ml \bullet \frac{Y}{100} \frac{mg}{ml} \quad (4)$$

Where Y is the concentration of the dye in the LSC-PM in ppm and X is the amount of used PDMS in grams, including the curing agent. This viscous dye-doped PDMS mixture is degassed in a desiccator to remove the ether and trapped gas (E+F). Both a 3D printed positive-relief 5.5x5.5 cm^2 mould of the channel structure and a petri dish are filled with the PDMS mixture and put *in vacuo* for 15 minutes (G+H+I). After 2 days of curing at room temperature (also 2h curing at 60 °C would be possible), the two layers of PDMS are exposed to plasma oxygen (30W, 30s, Emitech K1050X) and bounded together (J+K+L). The plates are cut into a 5x5 cm^2 reactor with the use of cutting blades (M+N) and 1/16" tubing is connected at the in- and outlet of the reactor by press and fit (O+P).

To obtain strong binding between the two plates with the use of plasma bonding, extremely smooth PDMS surfaces are needed. To create these smooth PDMS surfaces, a smooth mould surface is required. Therefore, the 3D-printed mould is printed on top of smooth HIPS plates with the use of HIPS filament. After removal of the cured PDMS from this mould, a smooth PDMS surface is created.

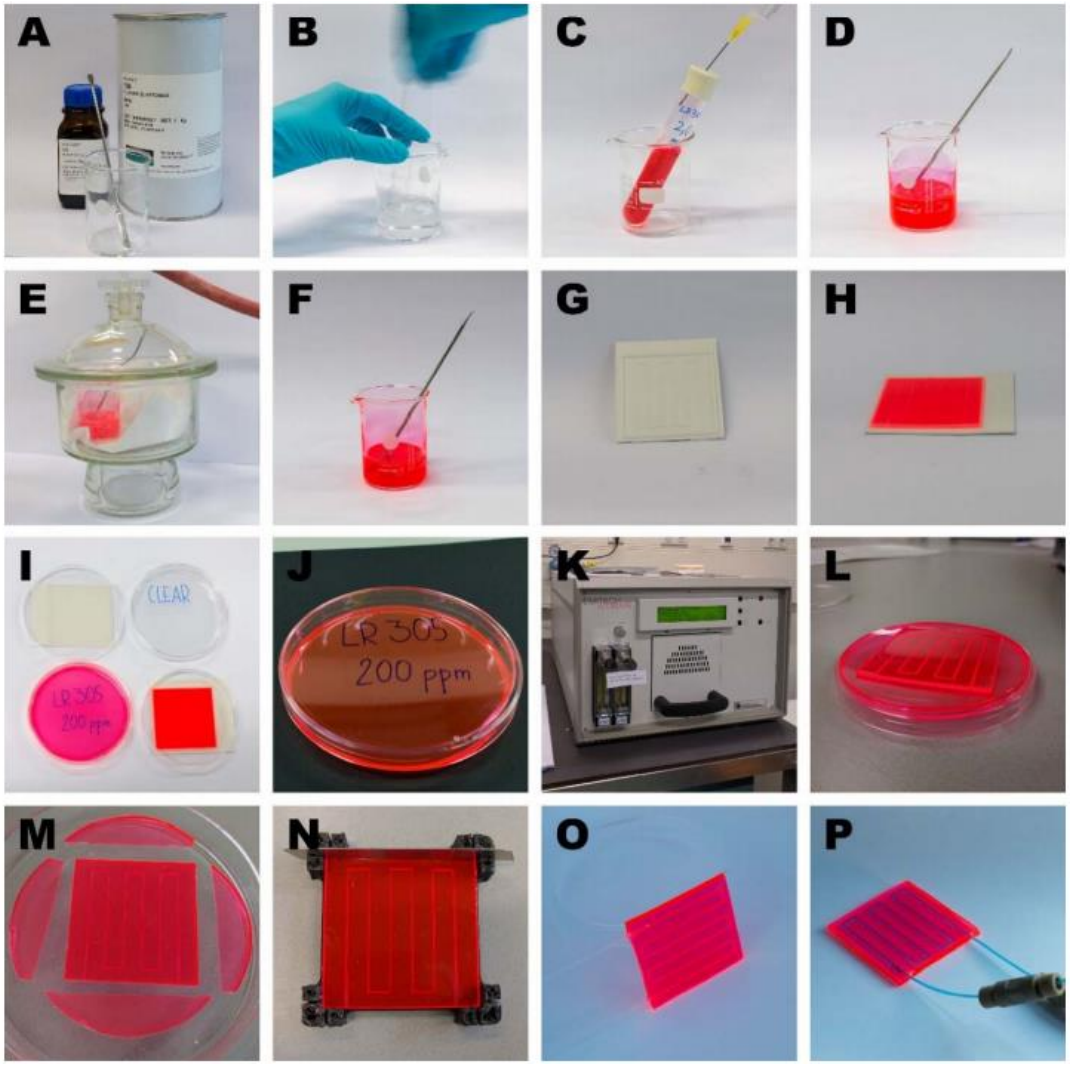

Figure 14: Production process of a PDMS based LSC-PM without the addition of capillaries. (Picture obtained from [1])

4.1.2 Production method with capillary

To add capillaries into the design of the reactor, a new production method is needed. In this method (see Figure 15), the shape of the 3D-printed mould is changed to fit the capillaries into a cured PDMS plate. In Chapter 4.1.3, different sized moulds will be discussed to fit the capillary. Once the PDMS is cured in this mould, capillaries will be put inside the cured PDMS slab and a second layer of uncured PDMS will be added on top of the cured PDMS. This second layer of PDMS will attach strongly to the cured layer of PDMS. After two days of curing at room temperature, the plate will be cut into a 5x5 cm^2 reactor using cutting blades.

It seems to be necessary to surround the channels/capillaries with at least 1 mm of PDMS to make the reactors rigid enough. Since the fitted capillaries have a larger outer diameter (1.6 mm) than the empty channels (1 mm), the newly designed reactors will have a slightly larger thickness (3.6 mm) than the LSC-PMs without capillaries (3 mm).

Since no plasma bonding step is present in this newly described production method, the need of smooth PDMS surfaces disappears. Therefore, a completely 3D printed mould could be used instead of using the smooth surface of the mould on the HIPS plate.

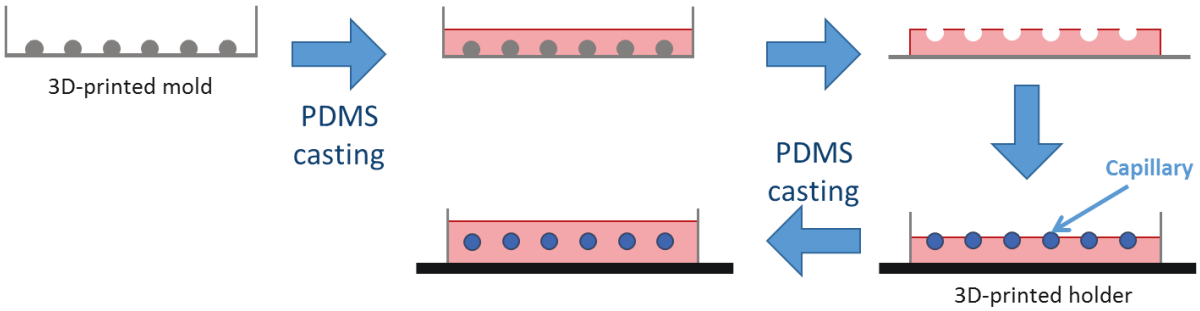

Figure 15: Schematic overview of the production process of the PDMS based LSC-PM with capillaries

4.1.3 Fitting capillaries

An effort has been made to create a 3D-printed mould which can produce a cured PDMS plate which is able to keep the capillaries into position. Several moulds were printed, while variating the angle, radius and depth of the design (see Figure 16). The angle was variated from 180° till 300°, the radius from 100% till 70% of the outer diameter of the tubing (1/16") and the depth from 0 mm till 0.8 mm.

Larger angles resulted in a stronger fitting of the tubing, but also made it harder to put the capillaries into the cured plate, since the opening in the PDMS plate was smaller. Using a bit smaller radius could reduce the amount of air bubbles trapped between the capillary and the PDMS. However, too small radii prevented the capillaries to fit into the plate. A certain depth was needed to keep the tubing into position. However, larger depths resulted in the use of a much thinner second layer of PDMS. This made an equal distribution of the top layer more difficult.

It was found that a good fitting of the capillary into the PDMS plate could be achieved when using an angle of 300°, a radius of 95% of the OD of the capillary and a depth of 0.5 mm. These conditions resulted in a PDMS plate with a significant smaller opening for the capillary (0.75 mm) than the OD of the tubing (1.6 mm). This did however not create any problems, due to the flexible character of the PDMS. When using these conditions, it was also possible to place the capillaries into more exotic shapes which could create more tension inside the plate, such as a half circle shaped design.

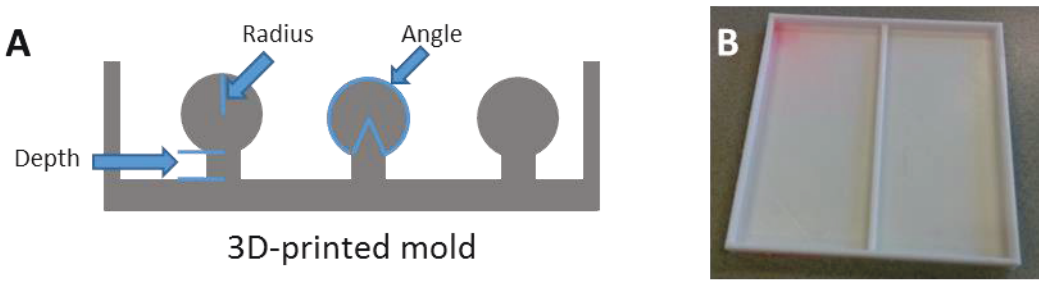

Figure 16 A) Schematic overview of the variated depth (0-0.8 mm), radius (100% - 70% of the OD of the tubing) and angle (180° - 300°) in the 3D printed moulds, B) 3D printed mould (depth: 0.5 mm; radius: 95%; angle: 300°) to produce the desired PDMS plates

4.1.4 Holder designs

When adding the second layer of PDMS, it is important to keep the first cured PDMS plate into position. If the newly casted PDMS can flow under the already cured plate a non-uniform reactor, which is thicker at the bottom than on the top, is created. It is also important to place the ends of the tubing out of the PDMS and the rest of the capillary below the surface of the newly casted PDMS layer. To create these circumstances, different 3D printed holders were designed to keep the cured plate in position, while the second layer of PDMS was added.

Firstly, a squared holder (see Figure 17A) was designed to keep the second layer of PDMS on top of the cured PDMS plate. This however led to a lot of leakage of the PDMS since there was no strong attachment between the holder and the cured PDMS plate. In another attempt, a completely 3D printed PLA holder was designed to keep the plate into position (see Figure 17B). Since this holder however exactly fitted the already cured PDMS plate, air bubbles easily got trapped under the cured PDMS plate during the degassing. As a result a lot of newly casted PDMS could easily flow under the cured PDMS plate resulting in a rough, now-uniform reactor (see Figure 17C). Increasing the size of the holder prevented the formation of the large air bubbles, but the cured PDMS plate still lifted from the bottom of the holder. To prevent the lifting, a good addition between the bottom of the holder and the cured PDMS plate was necessary. It was found that the PDMS could quite strongly attach to the smooth surface of a HIPS plate, which could prevent the second layer of PDMS flowing under the cured PDMS plate. The holders printed on the smooth HIPS plates (see Figure 17D) were able to keep the capillary into the PDMS, the ends of the tubing out of the PDMS and prevented lifting from the cured PDMS plate. This made it possible to create uniform LSC-PMs.

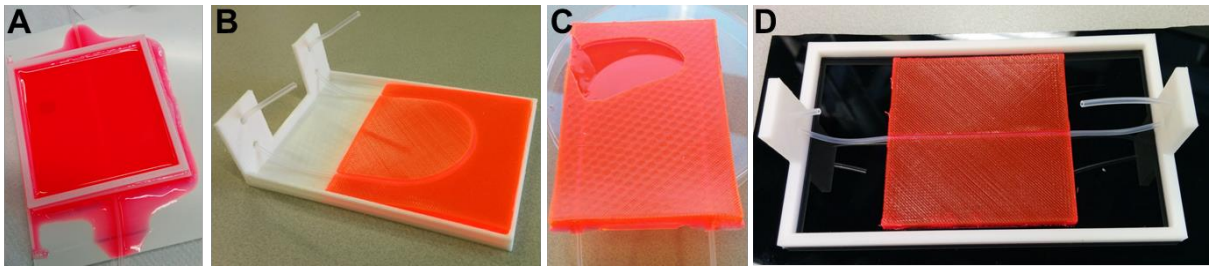

Figure 17: Several holder designs. A) A squared holder on top of a cured PDMS plate, B) A completely PLA 3D-printed holder, C) A destroyed PDMS plate due to trapped gas bubbles and newly casted PDMS lifting the plate, D) 3D-printed holder on top of a smooth HIPS plate

4.2 System overview

Once a reliable production method was developed, different capillaries have been tested into the LSC-PM. As been mentioned in chapter 2.3.1, the refractive index (RI) of a material can play a very important role in the light transport. Two different fluoropolymer tubing materials with different refractive indexes, PFA and Tefzel, have therefore been tested. Besides variating the tubing material, also the tubing dimensions were variated. The outer diameter of the tubing was kept constant on 1/16" (1.6 mm), while the inner diameter was variated from 0.01" till 0.04" (250 µm, 500 µm, 750 µm and 1000 µm). With these tests, the effect of a thicker tubing wall and a smaller reaction mixture penetration depth could be tested. Figure 18 shows a schematic overview of the different tested systems. For the matrix, 200 ppm LR305 doped PDMS is used (5.0x5.0x0.36 cm).

PFA is a well-known tubing material for photochemical applications in microreactor technology, because of its excellent optical properties towards both near-UV and visible light and good chemical stability[4]. Despite the good chemical stability, it was shown that plasticizer could leach from normal purity PFA[26]. To overcome this problem, high purity PFA tubing was used. This could avoid the possible contamination of the reaction mixture or the curing PDMS. PFA has a relatively low refractive index of 1.340.

Although the transparency of Tefzel tubing is a bit lower than the transparency of the PFA tubing, it is still quite high (transmittance ranging from 91% – 95%[27]). Furthermore, the oxygen permeability of Tefzel tubing (100 cm^3/100 in^2 24 h atm mil^{-1}) is significantly lower than the permeability of PFA (881 cm^3/100 in^2 24 h atm mil^{-1}) [28]. The refractive index of the Tefzel tubing is 1.400, which is closer to the refractive index of PDMS (1.41)[29]. All the needed capillaries were purchased from IDEX health & Science.

Light limited reactions can occur in different reaction mixtures. The refractive index of these reaction mixtures is assumed to be determined by the refractive index of the used solvent. Although, this approximation can be justified at low substrate concentrations (which is the case in this research, see chapter 4.3), it becomes less strong at higher concentrations. The use of different solvents results therefore in reaction mixtures with different refractive indexes. It is expected that light can reach a reaction mixture more easily, when using solvents with high refractive indexes. However, in most cases the solvent will be chosen depending on the reaction conditions instead of on its refractive index. Since the aim is to produce a LSC-PM which is able to accelerated a wide variety of reactions with different reaction mixtures, the reactors are tested with a solvent with a relatively low refractive index, namely acetonitrile (RI: 1.34). Once it is proven that reactions can be accelerated with a low refractive index solvent, other solvent systems will perform probably at least as good.

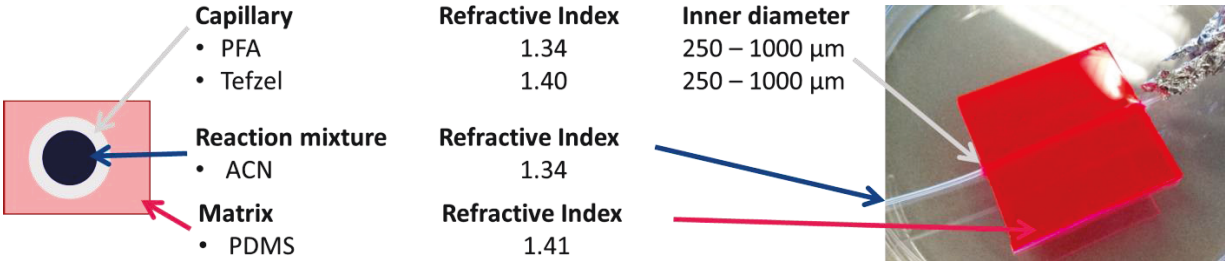

Figure 18: Schematic overview of the LSC-PM

4.3 Oxygenation of 1,9-diphenylantracene (DPA)

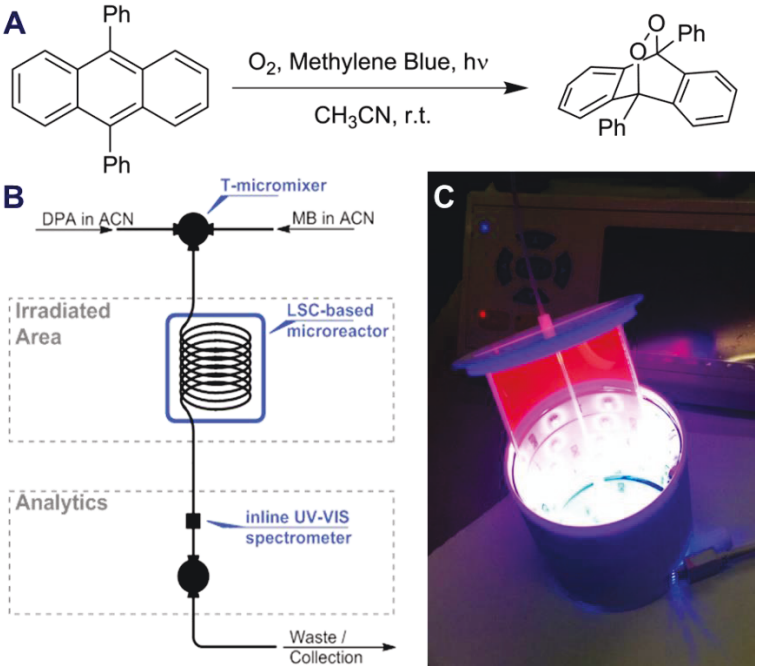

Figure 19: A) [4+2] cycloaddition of 1,9-diphenylanthracene with singlet oxygen, B) Schematic overview of the set-up, C) Picture of the used blue LED reactor with a red dye doped LSC-PM

To test and compare the different reactors described in the previous chapter (4.2), a test reaction was needed. The singlet-oxygen mediated photo oxygenation of 1,9-diphenylantracene (DPA) (see Figure 19A), was chosen because of the light-limited nature of the reaction kinetics. This reaction was described earlier with the use of $Ru(bpy)_3Cl_2$ as photocatalyst[30]. However, inside the LSC-PM methylene blue will be used as photocatalyst, due to the good absorption overlap with the emission spectrum of the dispersed fluorescent red dye. The oxygenation of DPA was particularly appealing as the decrease of the absorption peak of the starting material could be measured with an inline UV-VIS spectrometer (AvaSpec-ULS2048L, Avantes BV) to monitor the reaction conversion.

For the oxygenation of DPA, two 50 ml stock solutions of 0.4 mM methylene blue and 0.2 mM DPA in acetonitrile were prepared. The DPA stock solution was kept under argon in the dark. The methylene blue solution was saturated with oxygen, by bubbling of compressed air and kept in the dark afterwards. The two solutions were loaded into two syringes, which were connected via capillaries to a T-micromixer (see Figure 19B). The DPA solution in the syringe and in the capillary was kept in the dark by wrapped aluminium foil. Also the capillaries containing the reaction mixture before and after the LSC-PM were wrapped to prevent reaction outside of the LSC-PM. After the T-micromixer, the reaction mixture was lead through the LSC-PM towards the inline UV-VIS spectrometer, to monitor the absorption peak of the starting material. The absorbance at 0% conversion was measured by keeping the reaction mixture in the dark. The full conversion was measured after at least 30 minutes of direct irradiation of the reaction mixture.

The relative amount of starting material (DPA) inside the reaction mixture can be monitored by an absorption peak around 372 nm using the UV-VIS spectrometer. Conversion of the DPA results in a lower concentration of starting material in the reaction mixture and consequently a lower peak area at 372 nm in the spectrum. The conversion of the reaction could therefore be followed using the areas of the absorption peaks of the starting material at 372 nm with use of the following formula:

$$Conversion(\%) = \left(1 - \frac{Abs(x) - Abs(full)}{Abs(0) - Abs(full)}\right) \bullet 100\% \quad \textbf{(5)}$$

The LSC-PM was put inside a cylinder filled with blue LEDs and cooled with compressed air (see Figure 19C). Blue LEDs were used since there is a complete mismatch with the blue LED emission spectrum and the absorption spectrum of methylene blue. Therefore, down conversion of the light by the LSC-PM was necessary to perform the reaction.

4.4 Comparison of different capillaries

To examine the light limited reaction kinetics of the oxygenation of DPA in the LSC-PM, the reaction was performed under different light intensities of the blue LED. The reaction was performed at full intensity of the blue LED (12V), half intensity (10.15V) and 25% of the light intensity (9.22V) in a red doped LSC-PM with PFA HP (ID: 750µm) tubing. Appendix II shows the relation between the light intensities of the blue LED and the used voltages. It could be seen in Graph 4 that lower light intensities required longer residence times to achieve the same conversion, proving the light limited reaction kinetics at these conditions. The comparison of the different reactor systems will be done at low light intensities (9.22 V), since the differences in efficiency of the LSC-PMs are more visible, due to the slower reaction kinetics.

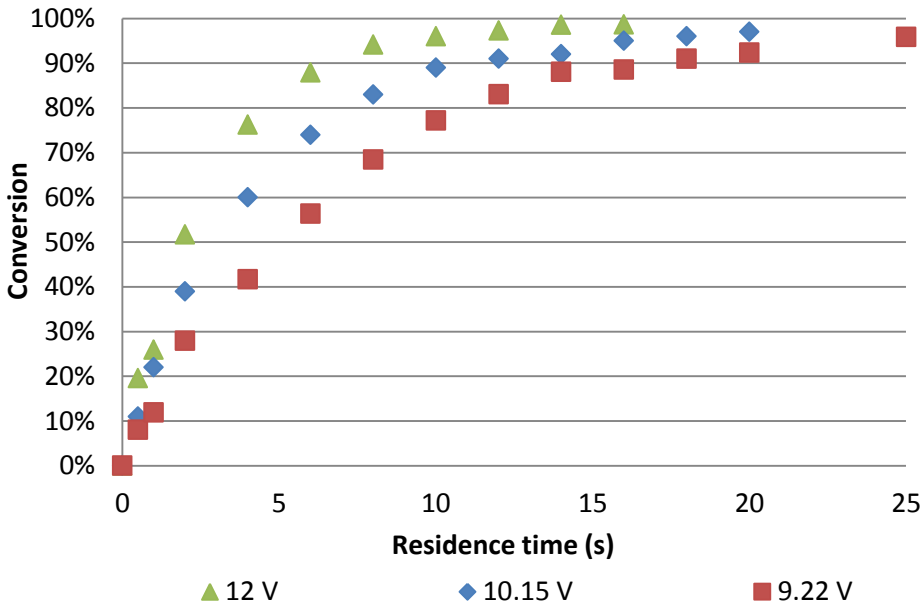

Graph 4: Conversion measurements (oxygenation of DPA) inside a LR305 doped PDMS based LSC-PM (200 ppm) with PFA HP (ID: 750 µm) tubing at different light intensities of the blue LED. [MB: 0.2 mM]

Variating the inner diameter of the tubing resulted in a clear trend (see Graph 5). It can be seen that smaller inner diameters perform significantly better than larger inner diameter. This effect could be caused by limitations of the light penetration through the reaction mixture. This will be discussed and investigated in more detail in chapter 4.5. Besides this, the trend of the Tefzel tubing seems to perform slightly better than the PFA tubing at all different inner diameters. This is likely to be caused by the higher refractive index of the Tefzel tubing which lowers the reflection of light moving from the PDMS matrix towards the tubing.

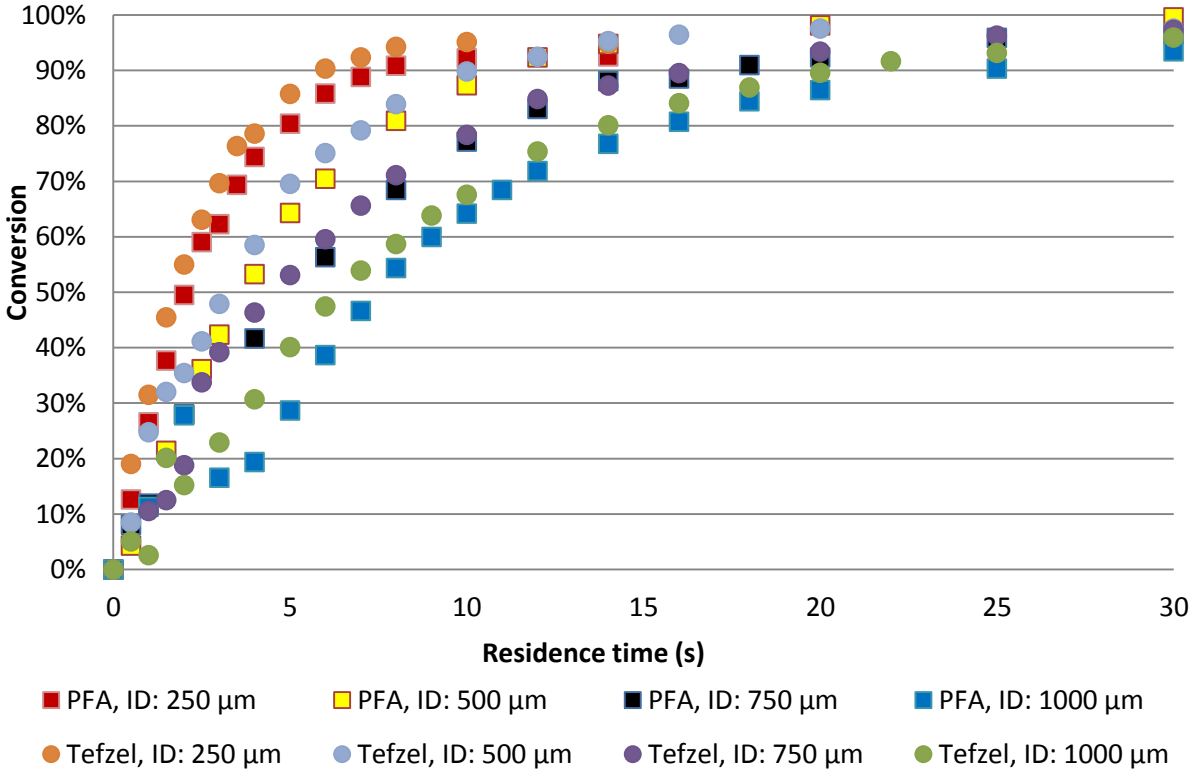

Graph 5: Conversion measurements (oxygenation of DPA) inside LR305-doped PDMS based LSC-PMs (200 ppm) with Tefzel or HP PFA tubing of different inner diameters [Blue LED: 9.22 V, MB: 0.2 mM]

4.5 Light penetration limitations

As shown in Graph 5, smaller inner diameter tubing performed significantly better than larger inner diameters. It was thought that this could be caused by limited light penetration through the reaction mixture inside the larger inner diameter tubing. When high concentrations of photocatalyst and large inner diameters are used, a lot of light is absorbed at the outside of the reaction mixture in the tube. Due to the high amount of absorptions, the amount of light reaching the centre of the reaction mixture is significantly lower than the amount of incoming light (see Figure 1). This prevents a good homogenous energy distribution over the complete reaction mixture, resulting in lower conversions.

This hypothesis was first tested theoretically by use of the law of Beer-Lambert-Bouguer (see chapter 2.1.2). In this particular case, the length of the pathway (d) is equal to the inner radius of the capillary and the absorbing component is the photocatalyst methylene blue (ε: 94000 M^{-1} cm^{-1} [31]).

Table 1 shows that the theoretical amount of light reaching the centre of the reaction mixture in the current reaction conditions (0.2 mM MB) is significantly higher in the smaller inner diameter tubing compared to the larger inner diameter tubing. Since light enters the tubing from all directions, the calculations are made using the inner radius instead of the inner diameter. It was calculated that a 1:10 dilution of the MB solution (0.02 mM MB) would decrease the differences in light penetration between the different inner diameters largely. While at high MB concentration (0.2 mM) the difference between the light reaching the centre of respectively the 250 µm and 1000 µm inner diameter tubing was still a factor 5, this decreased to a factor of 1.2 at low MB concentrations (0.02 mM).

Table 1: Theoretical calculations of the amount of light traveling through a reaction mixture containing MB with use of the law of Beer-Lambert-Bouguer

Inner diameter (µm)	Theoretical amount of light reaching the centre of the tubing	
	0.2 mM MB	**0.02 mM MB**
250	58 %	95 %
500	33 %	90 %
750	19 %	85 %
1000	11 %	80 %

Lowering the methylene blue concentration would besides increasing the transmission also decrease the catalytic activity. Experimentally, different concentrations of MB (variating from 0.2 mM to 0.01 mM) were tested in both 250 µm and 1000 µm Tefzel tubing at a fixed residence time of 4 seconds. Graph 6 shows a clear decrease in the catalytic activity in the 250 µm tubing, while the conversion in the 1000 µm tubing kept quite constant due to the opposite effects of the increased light transmission and the decreased catalytic activity. Although the trend is quite rough, it can be seen that at a methylene blue concentration of 0.02 mM the performances of both capillaries are in the same range. To test this statement, all four sized Tefzel tubing LSC-PMs were re-measured with a methylene blue concentration of 0.02 mM (see Graph 7). Due to the lowering of the catalytic activity, longer residence times were needed. To stay within the same time range as previous measurements, higher light intensities were used (12 V). A test at lower light intensity proved that the reaction was still light limited at these conditions.

It can be seen (Graph 7) that, at lower methylene blue concentrations, all four LSC-PMs with different sized Tefzel capillaries performed roughly the same. It was found that the Tefzel tubing (ID: 750 µm) also at these conditions outperformed the PFA tubing. To check whether addition of the capillary negatively affected the performances of the LSC-PM, these results were compared with a LSC-PM without capillary. This reactor contained a rectangular reaction channel of 1.0x0.35 mm. It was found, that the performances of all reactors were in the same range, proving that the addition of capillaries did not have a significant effect on the performances of the reactor.

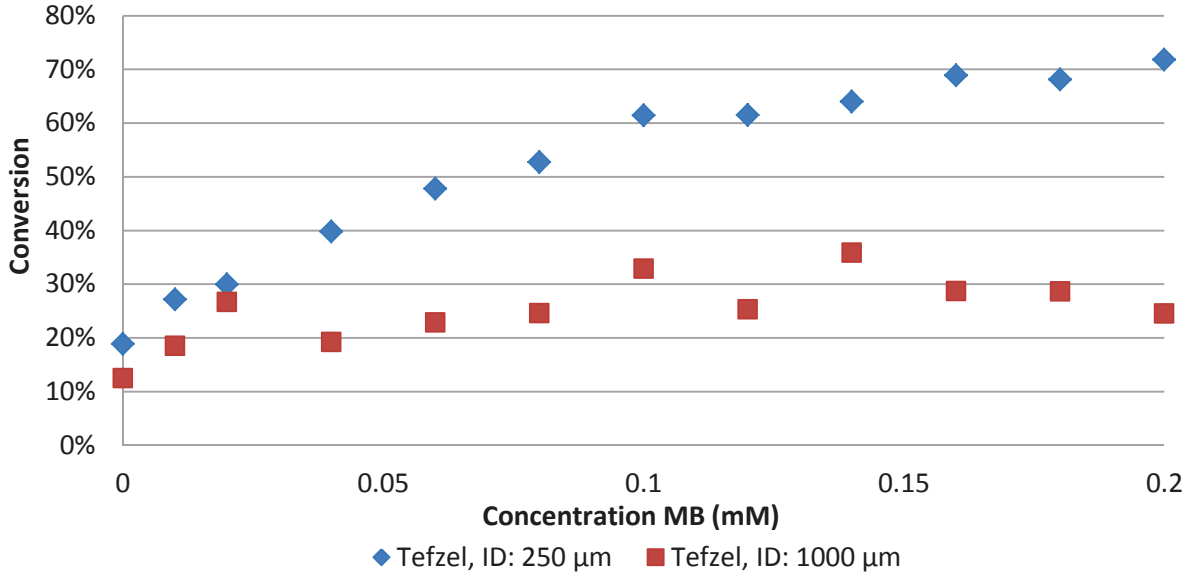

Graph 6: Conversion measurements (oxygenation of DPA) inside LR305-doped PDMS based LSC-PMs (200 ppm) with Tefzel tubing (ID: 250 µm and 1000 µm) at different methylene blue concentrations after a residence time of 4 seconds [Blue LED: 9.22 V]

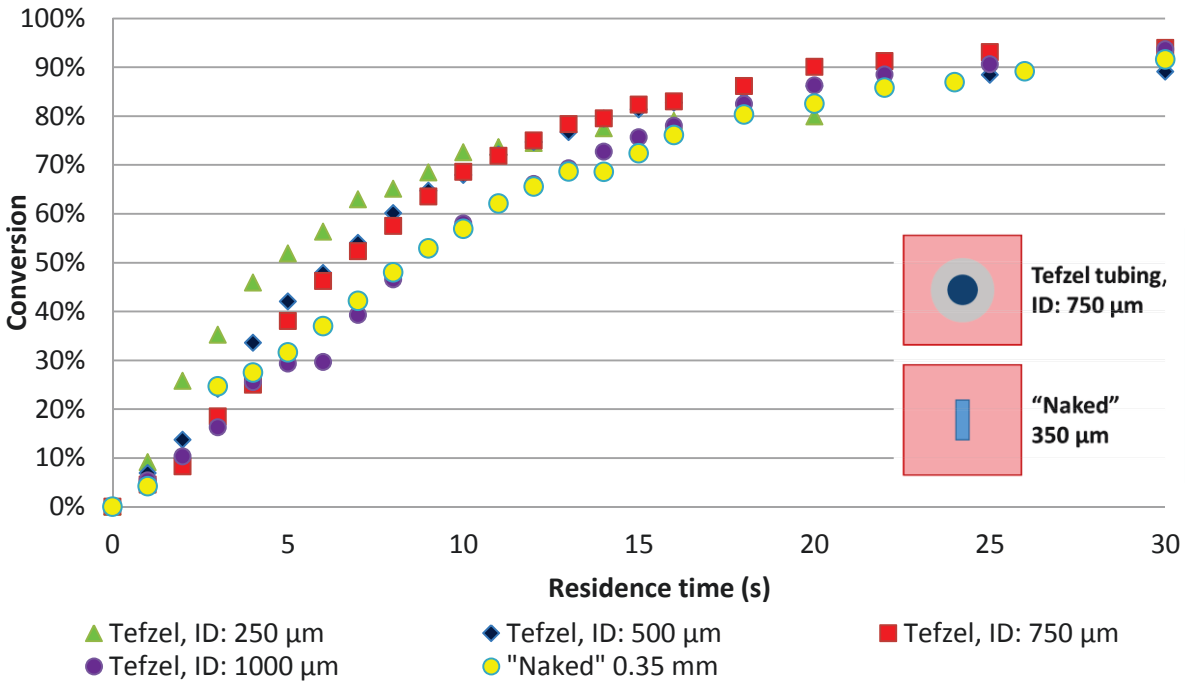

Graph 7: Conversion measurements (oxygenation of DPA) inside LR305-doped PDMS based LSC-PMs (200 ppm) with different inner diameter Tefzel tubing and without capillary [Blue LED: 12 V, MB: 0.02 mM]

4.6 Scaling up

To be able to perform photochemical reactions which need longer residence times and to increase the throughput of the LSC-PM, an attempt was made to scale up the reactor. A mould was produced with 5 half circles (see Figure 20B), creating a reactor volume increase of more than 7 times compared to the previous design. However, the large sizes of the reactor resulted in the formation of a lot of air bubbles and in newly casted PDMS flowing under the plate resulting in a destroyed non-uniform reactor (see Figure 20A). Scaling up with the current production method is quite difficult, due to the manufacturing issues encountered by the larger sizes of the PDMS layers.

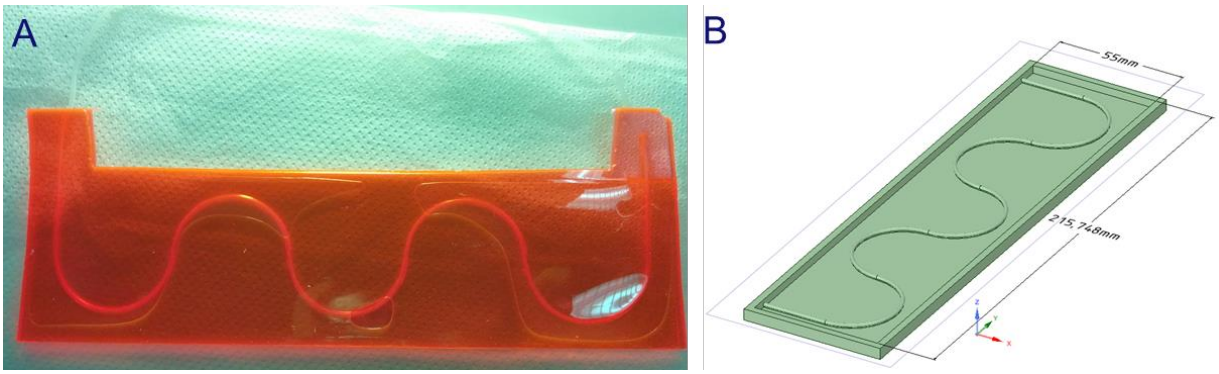

Figure 20: A) Destroyed scaled-up LSC-PM due to lifting and air bubbles, B) Design of the 3D-printed mould for the scaled up reactor.

5 Polymethyl methacrylate (PMMA)

Since several drawbacks occur when using PDMS based devices (see chapter 3), a different polymeric material, namely polymethyl methacrylate (PMMA), is investigated as alternative polymeric matrix for the dye dispersion. In this chapter, a theoretical and experimental comparison between both matrices is made. Furthermore, effort has been made to scale up the reactor and to check the influence of the PMMA addition. Lastly, different coloured PMMA plates have been investigated.

5.1 Theoretical comparison of PMMA vs. PDMS

Producing the LSC-PM with PMMA has several advantages over the use of PDMS. In this chapter the different advantages will be discussed in more detail.

5.1.1 Refractive index

One of the main advantages of PMMA is the significant higher refractive index of the material (RI: 1.49)[32] compared to PDMS (RI: 1.41)[29]. This higher refractive index could theoretically increase the amount of light reaching the reaction mixture due to an increase of total internal reflections and consequently a decrease in the losses via the escape cone (see chapter 2.3). Therefore, a PMMA based LSC-PM could be even more efficient than a PDMS based reactor.

5.1.2 Dye stability

It is known that after a period of 17 years of sunlight irradiation the performances of the PMMA matrix are still close to the original performances[33]. Since there is no significant decrease in the performances of the PMMA, the limiting factor could be the degradation of the Lumogen Red 305 dye in the PMMA matrix. Vanmaekelberg and co-workers[34] showed that the degradation of the dye is depended on the used dye and on the matrix material (see Graph 8). They showed that the absorption of the LR305 dye in PMMA plates only decreased with 3% after outdoor solar irradiation of 85 weeks. Compared to the rapid decrease of the absorption in the PDMS matrix (56% after 78 weeks, see Chapter 3.4), a PMMA matrix could extensively extend the lifetime of the LSC-PM.

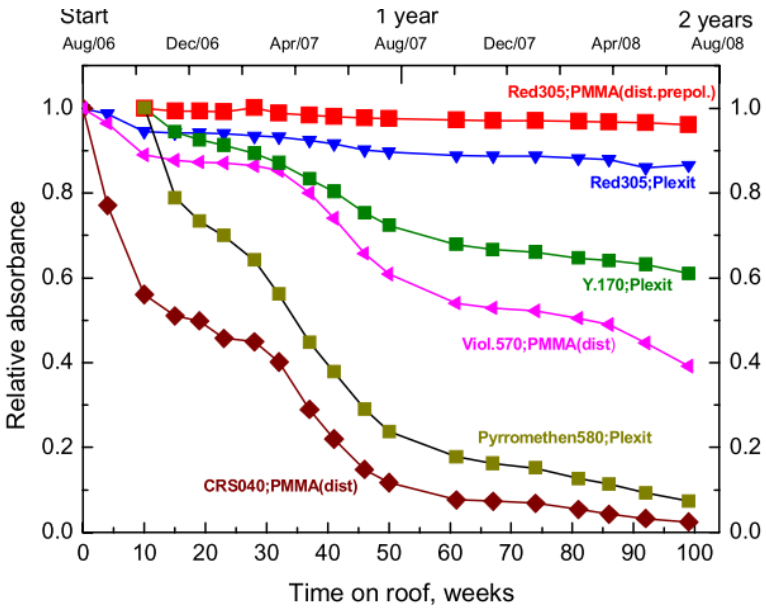

Graph 8: Relative absorbance of different dyes in different polymer matrices as a function of time under outdoor irradiation conditions. (Picture obtained from [34])

5.1.3 Luminophore compatibility

Due to the more polar structure of PMMA, more fluorescent dyes can be dissolved at higher doping concentrations inside the matrix compared to the PDMS matrix. A lot of fluorescent coloured plates are commercially available[35–37], which creates a lot of possibilities for photochemical reactions with other photocatalysts (see chapter 2.4.1). These plates are mostly known under their trade name "Plexiglas".

5.1.4 Price

The price of PMMA is significantly lower than the price of PDMS. A mixture of both the PDMS base and initiator (Dow Corning Sylgard 184) has a price of €280 per kg (270 k€/m^3), which is almost a factor of 20 higher than the price of commercial fluorescent Plexiglas (PMMA) plates (€13/kg; 15.6 k€/m^3). It should be noted that this comparison could be an underestimation, since the manufacturing costs of the PMMA sheets are included in this price, while this is not the case for the PDMS base and initiator mixture. Both prices are based on a quote from a supplier. The PDMS is purchased from MAVOM Chemical Solutions and the PMMA is purchased from Limacryl.

5.1.5 Mechanical properties

Since the flexible character and the low tensile strength (6.7 MPa[29]) of PDMS made the LSC-PM very fragile, a more rigid material would be desired. PMMA does not have a flexible character and has a factor of 10 higher tensile strength (48 - 76 MPA[32]), creating a much more rigid LSC-PM.

5.1.6 Availability

PMMA plates are frequently used for example for designing purposes under their tradename "Plexiglas". This frequent use offers several advantages. Firstly, large productions are present due to the large demand, which creates an availability of a lot of different fluorescent coloured PMMA plates. Furthermore, the large market results in a lot of knowledge and frequent research over the material. For example the degradation of the dyes inside the plates or the stability of different coloured plates has been intensively studied.

5.2 Production method

Producing PMMA LSC plates creates several challenges. To create a PMMA plate, the MMA mixture must be thermally polymerized in a water bath of 50 °C during 20 hours[34]. Since the volume of the mixture shrinks significantly during this polymerization step, the mixture must be placed between two vertically oriented glass plates which are separated by an elastic distance holder[38]. The slow polymerization rate and the elastic character of the holder should prevent undesirable partial separation and formation of air bubbles inside the PMMA plate. After the polymerization in the water bath of 50 °C, a post-treatment at 110 – 120 °C is needed to remove the remaining monomer[34].

Since producing PMMA plates on lab-scale is quite challenging and since the availability of fluorescent doped cheap PMMA plates is sufficient, PMMA plates were purchased commercially. 3 mm thick plates were ordered from Evonik (PLEXIGLAS Fluorescent Bright Red 3C02 GT) and 4 mm thick custom made plates were ordered from Limacryl. The 4 mm thick Limacryl plates contained 100 ppm Lumogen F Red 305. By use of UV-VIS measurements of both plates, it could be shown that the Evonik plate contained approximately 115 ppm of Lumogen F red 305 (see Appendix III). The same Evonik plates have been used in previous LSC research[39].

To be able to add capillaries into the purchased PMMA plates, small holes were drilled into these plates. Firstly, a 2.0 mm hole with a length of 5 cm was drilled into the Evonik plate. Because of the length of the drill, the depth of the hole is limited to 5 cm. Due to the relative large dimensions of the hole (2.0 mm) compared to the outer diameter of the tubing (1.6 mm), the inserted capillary could easily move through the drilled hole. To create a stronger fitting of the capillaries, the dimensions of the hole were decreased to 1.6 mm. Due to the comparable dimensions, pushing the capillary through the hole was very difficult. This pushing led to thickening and bending of the capillary. Pulling the capillary through the hole resulted however in a strong fitting of the tubing inside the plate. In that case, the end of the capillary was thinned (either by cutting or stretching) and pushed through the hole. Once the thin end of the tubing was through the plate, the rest of the capillary was pulled through, creating a PMMA based LSC-PM (see Figure 21).

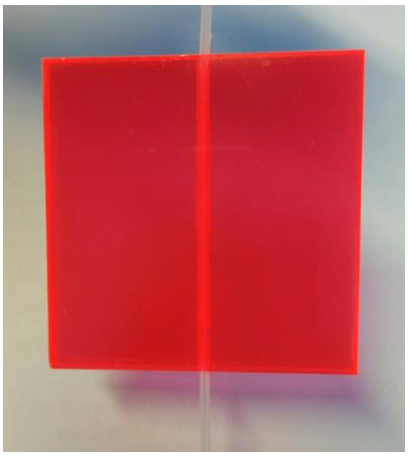

Figure 21: Red PMMA based LSC-PM

5.3 Experimental comparison of PMMA vs. PDMS

To see the influence of the use of PMMA instead of PDMS on the performances of the LSC-PMs, a direct comparison was needed. Firstly, the edge emission of both a red dye doped PDMS (125 ppm) and PMMA (115 ppm) plate was measured. For these measurements, the 50x50x3 mm plates were put onto a holder, which was connected to an integrating sphere (LMS 1050). The top of the plates was irradiated by a solar simulator (LS0110-100, L.O.T.). This light was transferred to the edges of the plates and the light flux coming from the edges was consequently measured by the integrating sphere (see Figure 22). The light flux was measured in W/nm. Since photons at shorter wavelengths contain a higher amount of energy, a transformation from the light flux towards the amount of photons is needed to make a fair comparison. The calculation of the photon flux (φ_{ph} [mol (nm s)$^{-1}$]) could be done as follows by use of the light flux (φ_{light} [W/nm]), the Avogadro number (N_A [mol^{-1}]), the Planck constant (h [J s]), the wavelength (λ [m]) and the speed of light (c [m/s]):

$$\varphi_{ph} = \frac{\varphi_{light}}{N_A h} \cdot \frac{\lambda}{c} \qquad (6)$$

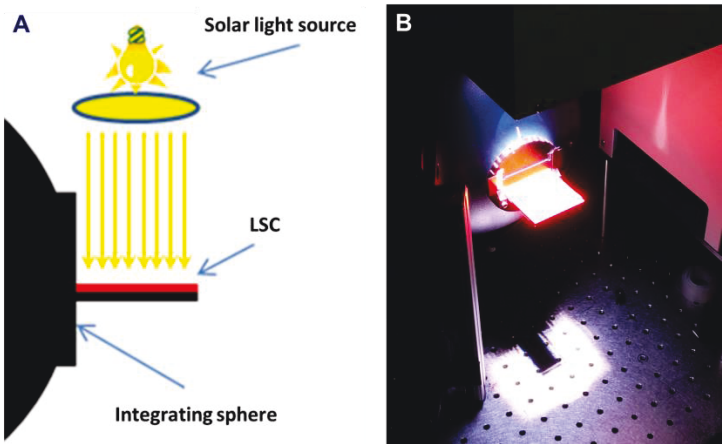

Figure 22: Schematic overview (A) and picture (B) of the edge emission measurement set-up

Graph 9 clearly shows the difference between the edge emission of the PMMA and the PDMS plate. Although the dye doping of the two plates differs slightly (less than 10%), still some conclusions can be drawn from this graph. It can be seen that, due to the higher refractive index of PMMA, more light is transported towards the edges of the plate. This could increase the performances of the LSC-PM, since in that case more light will be transported towards the reaction channels. Furthermore, the two peaks are at a slightly different position. Apparently, the different matrix materials slightly influence the position of the emission peak of the red dye.

To compare the performances of the two materials inside a LSC-PM, two identical reactors in both matrixes were produced. Since the smallest thickness of a PDMS based LSC-PM is 3.6 mm, thicker PMMA plates than 3 mm were needed. Therefore, some custom-made LR305 doped (100 ppm) 4 mm thick PMMA plates were purchased. The conversion measurements of the oxygenation of DPA in both the PDMS and the PMMA reactor (50x50x4 mm, 100 ppm) are shown in Graph 10. It can be seen that the PMMA based reactor significantly outperforms the PDMS reactor since shorter residence times are needed to achieve the same conversion.

Also the Evonik PMMA based reactor, which is thinner (3 mm) and has a higher dye loading (115 ppm), was tested. Although the amount of dye per volume is higher inside the 3 mm Evonik PMMA plates, the total amount of dye is higher inside the 4 mm Limacryl PMMA plates, due to the larger thickness. A thicker plate could decrease the performances of the reactor due to a larger change of light, which is travelling through the reactor matrix, passing by the reaction channel (see Chapter 7.3, Figure 28). Different amounts of dye could also influence the performances. Higher dye loadings could result in a larger change to absorb light, but could also increase the light losses due to an increase of re-absorptions. The re-emitted light could be emitted towards the escape cone of the surface, which would result in escaping of the light. Graph 10 shows that these effects on these scales are negligible or level each other out.

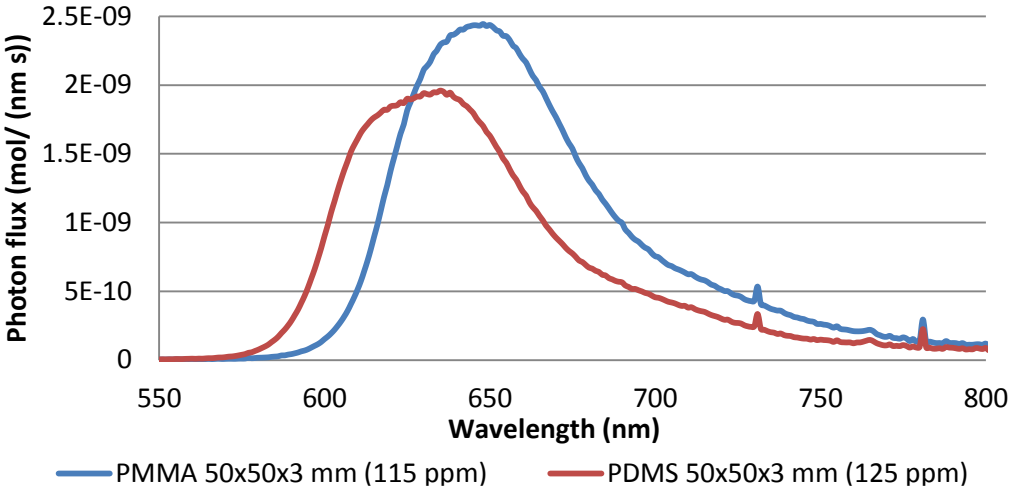

Graph 9: Edge emission of a red dye doped PMMA (115 ppm) and PDMS (125 ppm) plate of identical dimensions.

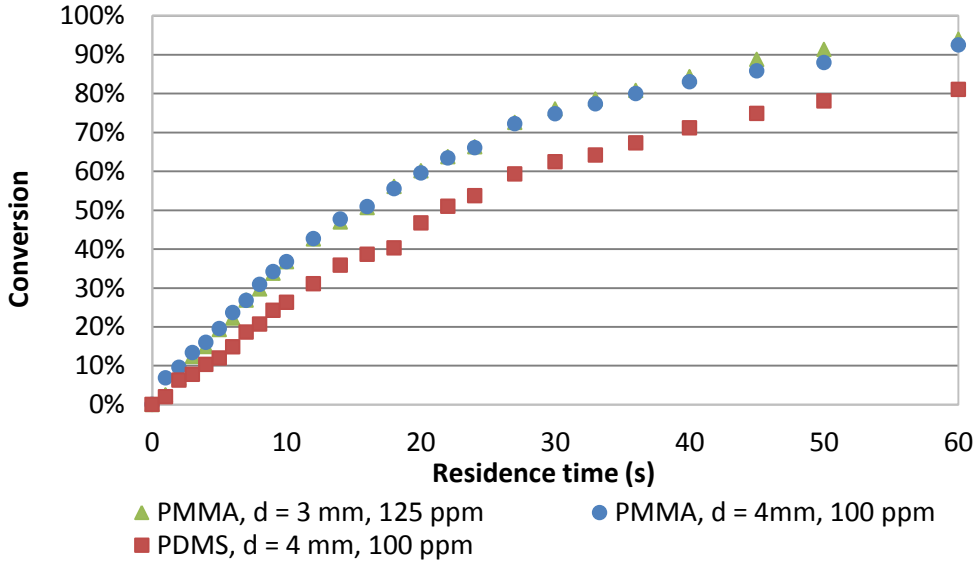

Graph 10: Conversion measurements (oxygenation of DPA) inside LR305-doped PDMS and PMMA based LSC-PMs [Blue LED: 10.15 V, MB: 0.02 mM, PFA tubing ID: 750 µm]

5.4 Comparison of different capillaries

Since several capillaries with different refractive indexes resulted in different performances of the PDMS based LSC-PM (see chapter 4.4), also different tubing were tested in the PMMA based LSC-PM. Besides PFA HP (RI: 1.34) and Tefzel tubing (RI: 1.40), also Halar tubing was tested. Only a limited amount of examples of the use of Halar tubing in photochemistry is reported[28,40], compared to Tefzel and PFA tubing. Halar tubing is known for its high refractive index (1.447) and its extremely low oxygen permeability (25 100 $cm^3/100\ in^2$ 24 h atm mil^{-1})[28]. Beside this, Halar has a less flexible character than Tefzel and PFA tubing. Since IDEX Health & Science did not produce Halar tubing, the tubing was purchased from APT (Advanced Polymer Tubing).

It can be seen in Graph 11 that at a light intensity of 12V the different tubing materials performed almost equally (Graph 11, crosses). The oxygenation of DPA could possibly be out of the light limited regime of the reaction, due to the higher amount of light reaching the reaction channel inside the PMMA based reactor at this relatively high light intensity. Therefore, the reaction was redone at half of the light intensity (10.15 V). The lower light intensity significantly lowered the reaction rate, so the light limited character of the reaction was visible (Graph 11, triangles). However also at this lower light intensity, the performances of the different tubing materials were comparable.

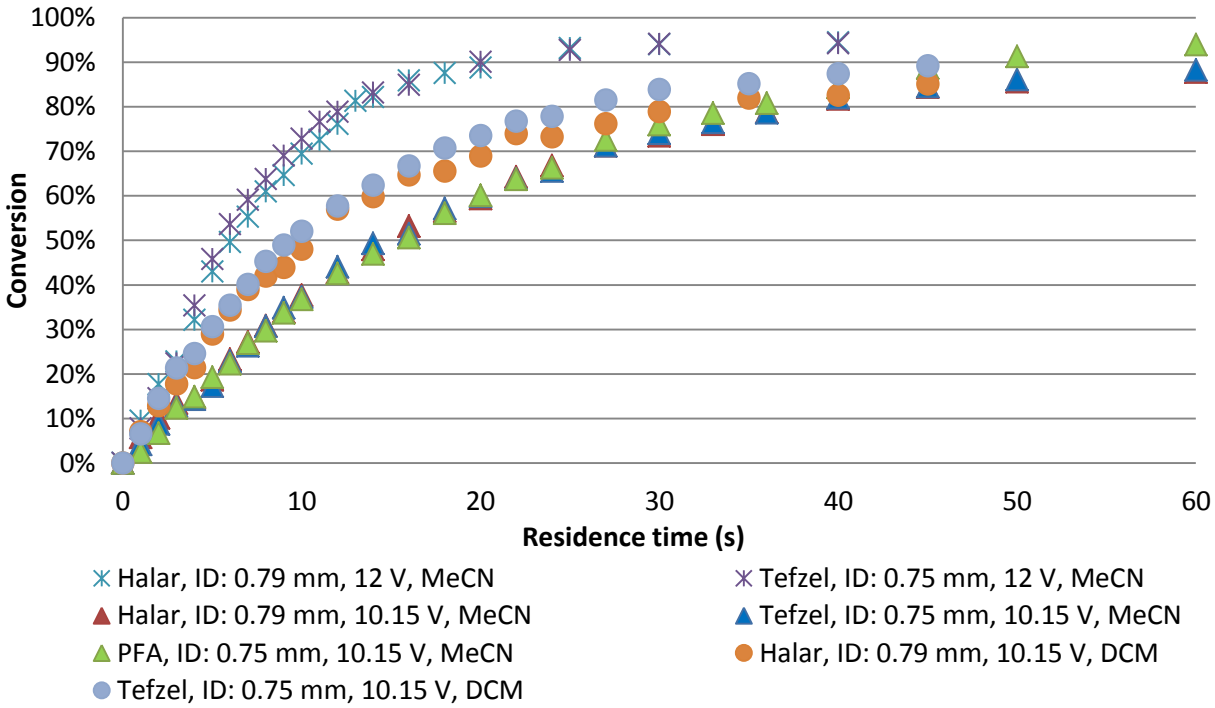

Graph 11: Conversion measurements (oxygenation of DPA in different solvent systems [MeCN and DCM]) in LR305-doped PMMA based LSC-PMs with different tubing materials (PFA, Tefzel and Halar) at different light intensities (12 V and 10.15 V) [Blue LED, MB: 0.02 mM]

The low refractive index of acetonitrile (RI: 1.34) could limit the reaction system as well. In that situation, the reaction would be limited by the refractive index of the solvent, instead of by the refractive index of the capillary. This could be another explanation for the comparable behaviour of the different capillaries. To test this hypothesis, an attempt was made to perform the oxygenation of DPA in other solvent systems, with a higher refractive index. Several problems occurred when using different solvents for the oxygenation of DPA (see Table 2).

Methylene blue was insoluble in toluene, which rejected the possibility to use toluene. When using DMSO or DMF, the DPA oxygenation did not occur. Performing the reaction in chloroform resulted in the slow formation of gas bubbles inside the UV-VIS flow cuvette under UV irradiation, which made it impossible to follow the reaction in a stable way. Lastly, DCM was tested, in which the reaction was performed successfully. Graph 11 shows that, although the reaction conditions are changed towards DCM, the performances of the different capillaries are still in the same range (Graph 11, circles). It can be concluded that variating between these tubing materials does not have a significant influence on the performances of the PMMA based LSC-PM.

Table 2: An attempt to perform the oxygenation of DPA in different solvent systems

Solvent	Refractive Index	Issue
Toluene	1.50	Methylene Blue doesn't dissolve
DMSO	1.48	No reaction
Chloroform	1.45	Gas formation inside the flow cuvette
DMF	1.43	No reaction
DCM	1.42	✓

5.5 Hydroxylation of arylboronic acids

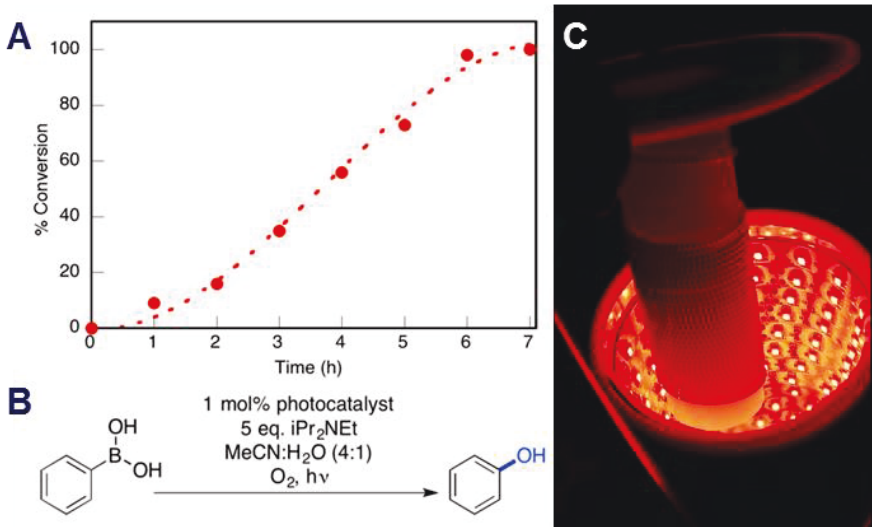

Figure 23: A) Conversion measurements of the hydroxylation of phenylboronicacid in batch with the use of an oxygen balloon (Picture obtained from [41]), B) The hydroxylation of phenylboronicacid, C) The used reactor for flow experiments (Halar tubing ID: 0.79 mm, V_R: 1.5 ml, Red LED)

Effort has been made to perform another methylene blue catalysed reaction inside the LSC-PM. Several examples of oxygenation, oxidation[42] and trifluoromethylation[43] photoredox reactions catalysed by methylene blue are known[10]. The methylene blue catalysed oxidative hydroxylation of arylboronic acids was investigated here in more detail. Previous research[41] showed that full conversion of phenylboronicacid towards phenol (Figure 23B) was achieved after 7 hours of reaction in batch (Figure 23A). The hydroxylation of 4-nitrophenylboronicacid instead of phenylboronicacid was chosen as a test reaction, since the addition of the nitro functional group made it possible to follow this reaction by UV-VIS. After running this reaction in batch with the use of an oxygen balloon following the described procedure[41], the reaction was performed in flow with the use of a red LED. The red LED was used to mimic the conditions inside a red doped LSC-PM.

Two separate solutions were prepared and put into two syringes. One contained the starting material (4-nitrophenylboronicacid, 1.2 mmol) in solution (MeCN:H_2O, 4:1, 10ml), while the other one contained the amine (DIPEA, 6 mmol) and the photocatalyst (MB, 0.012 mmol) in solution (MeCN:H_2O, 4:1, 10ml). The two solutions were brought together in the dark by use of two capillaries connected to a T-mixer. This combined liquid flow was transported through a capillary in the dark to a second T-mixer, which was connected to a gas flow. A gas to liquid ratio of 2:1 was used, which created a stable slug flow entering the reactor. The reactor was constructed out of 3.06 m Halar tubing (ID: 0.79 mm) with a total volume of 1.5 ml (see Figure 23C). The reaction was followed by UV-VIS measurements after a 1:500 dilution. The needed UV-VIS measurement of the full conversion was achieved by measuring a solution of commercially purchased 4-nitrophenol (TCI Chemicals).

Firstly, the light limited character of the reaction was proven by performing the reaction at different light intensities (12V, 9.5V and 8V) (see Table 3, row 3). Literature[41] stated that the use of oxygen instead of compressed air could increase the conversion. The influence of oxygen was also visible in the flow experiments, where higher conversion was achieved when using oxygen instead of compressed air (see Table 3, row 3). After a residence time of 30 minutes, 68% conversion was achieved (oxygen, 12V).

Table 3: Conversion measurements of the hydroxylation of 4-nitrophenylboronicacid in flow at different light intensities using a slug flow (G:L 2:1) with respectively compressed air or oxygen [Red LED, V_R: 1.5 ml]

	Residence time (min)	Compressed air (12V)	Oxygen (12V)	Oxygen (9.5V)	Oxygen (8V)
1	1	5 %			
2	5	18 %			
3	10	23 %	27 %	17 %	10 %
4	20		46 %		
5	30		68 %		

After several GC-FID measurements it was found that the purchased 4-nitrophenylboronicacid (TCI Chemicals) contained several contaminants. Therefore, the rest of the research was continued with the hydroxylation of phenylboronicacid (Figure 23B), which did not contain any contaminants and was much cheaper. Since it was no longer possible to follow the reaction by UV-VIS, the conversion was calculated by use of GC-FID measurements. Decafluorobiphenyl was added as internal standard to the starting material solution (0.5 equivalent of the starting material). A calibration curve was obtained ($N_{product}/N_{I\_S} = 2.2355\ A_{product}/A_{I\_S}$, R^2: 0.9998, where A is the peak area and N is the amount in mole) to convert the GC-FID measurements to conversions.

5.6 Scaling up

Since relatively long residence times were needed for the hydroxylation of phenylboronicacid, larger reactor volumes and consequently reactors were needed to perform the reaction inside a LSC-PM. Several red PMMA reactors were produced of respectively 10x10cm^2, 20x20cm^2 and 30x30cm^2 (see Figure 24). Several 5 cm Evonik red PMMA (115 ppm, 3 mm thickness) plates were connected to each other to create the larger reactors. Due to the limited length of the drill, separate plates of 5 cm were used. The holes were drilled with an inter channel spacing of 2.5 cm and PFA HP (ID: 750 µm) was used to connect the plates. This resulted in a reactor volume of respectively 180 µl, 730 µl and 1640 µl for the 10x10cm^2, 20x20cm^2 and 30x30cm^2 LSC-PMs. Since there was no clear difference between the performances of the tested capillaries (see chapter 5.4), HP PFA tubing was chosen for the reactors. This choice was made, because PFA is a frequently used tubing material in photochemistry and because of its flexible character, which made pulling the capillary through the plates easier. For the 10x10cm^2 and the 20x20cm^2 reactors also 3D printed holders were designed to keep the capillary into the same position as inside the reactor (see Figure 24). This made it possible to see the influence of the PMMA compared to the performances of a design without a polymeric matrix material.

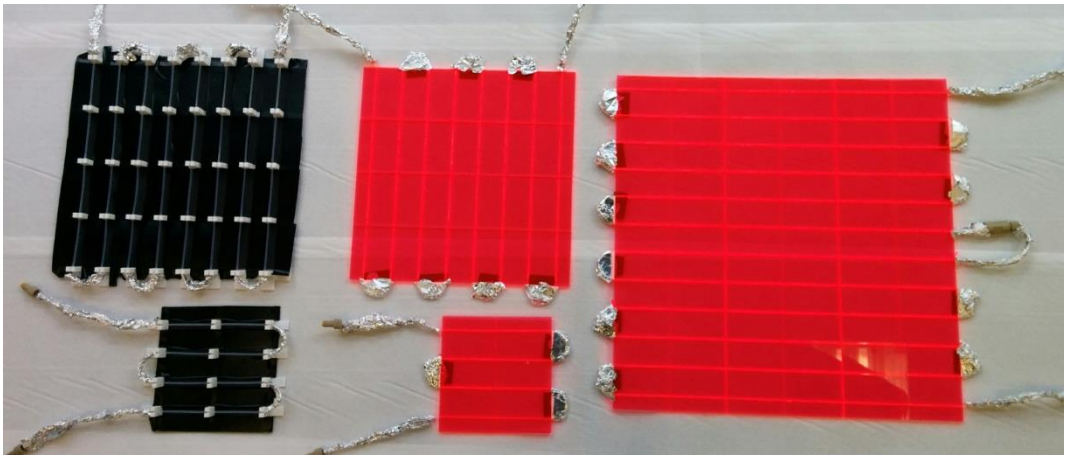

Figure 24: 3D printed holders (10x10cm^2, 20x20cm^2) to keep capillaries into position (left) and three scaled up red PMMA reactors (right) (10x10cm^2, 20x20cm^2 and 30x30cm^2)

The hydroxylation of phenylboronicacid was performed under a solar simulator (KHS Solar Constant 1200) in all five reactors (both with and without PMMA) to test the influence of the different sized reactors and the effect of the LSC-PM design. It was aimed to keep the temperature of the reactors constant by cooling with compressed air. An oxygen to liquid ratio of 3:1 was used and a back pressure regulator of 5 psi was placed after all reactors to prevent flushing of the reactor after a build-up of pressure. The conversion of the reaction was monitored by use of GC-FID measurements.

Graph 12 shows the conversion measurements of the hydroxylation of phenylboronicacid in the different reactors. The behaviour of both the clear 10x10cm^2 reactor (slope:0.002, R^2:0.986) and the clear 20x20cm^2 reactor (slope:0.0019, R^2:0.996) was quite comparable as expected. The increased performances of the LSC-PMs compared to the clear reactors can easily be noticed. Both the 10x10cm^2 and the 20x20cm^2 reactor performed more than two times as good as the clear reactors. Within the same residence time, the conversion inside the LSC-PMs is two times as high as the conversion inside the clear reactors. Furthermore, Graph 12 shows that full conversion of the reaction can be achieved within four minutes. This is a decrease in residence time of two orders of magnitude compared to the needed seven hours in batch[41].

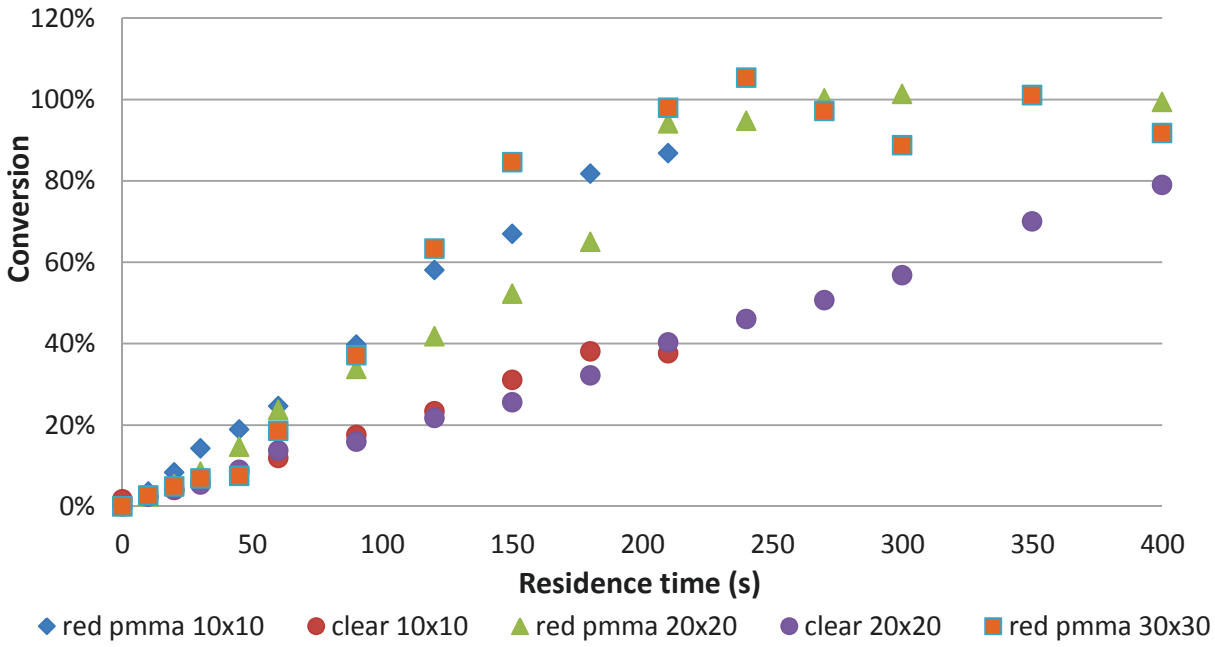

Graph 12: Conversion measurements of the hydroxylation of phenylboronicacid in different sized clear and red PMMA (Evonik, 3 mm, 115 ppm) reactors. The experiments were carried out under solar simulator conditions and the conversion was followed by the use of GC-FID

Although, a clear difference between the clear and the PMMA reactors is visible, there is still quite a broad variation in the performances of the different sized red PMMA LSC-PMs. No clear trend can be seen in those variations. It is thought that these variations can possibly occur due to variations in the residence time. Due to the relatively large pressure drop over the reactor and the consumption of oxygen by the reaction, the residence times could differ significantly compared to the set flow rates. It would be meaningful to test the residence times inside the different reactors by use of a tracer (see chapter 7.1).

The measurements in Graph 12 show at low conversions an upward curvature, which is contrary to the negative curvature which is normally observed. This same behaviour has also been observed in literature during batch experiments (see Figure 23A). This behaviour has been explained[41] by the fact that fewer triplets are quenched by phenol compared to phenylboronicacid. Therefore, more MB triplets survive to be quenched by DIPEA, when the concentration of starting material decreases. This effect causes a slight positive curve over time. Figure 25 shows the proposed reaction mechanism.

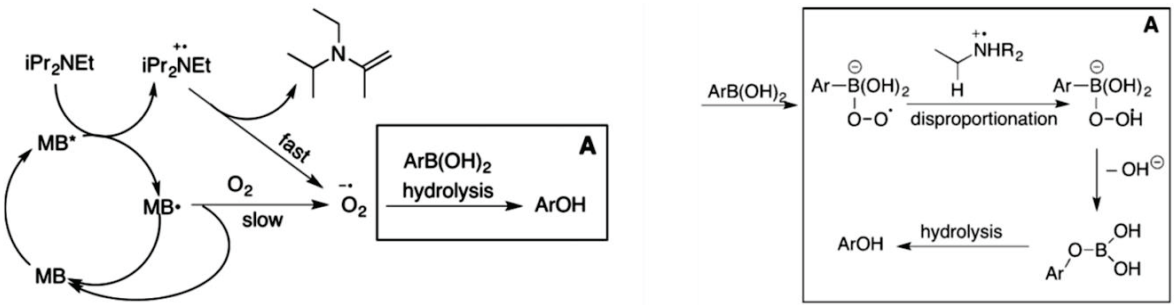

Figure 25: Proposed reaction mechanism for the oxidative hydroxylation of arylboronic acids as proposed by Xiao and co-workers[44] and Scaiano and co-workers[41]

5.7 Coloured plates

As explained in chapter 5.1.3 different fluorescent coloured PMMA plates can be purchased. When a good overlap is present between the emission spectra of these coloured plates and the absorption spectra of a photocatalyst, new reaction systems could be tested. To investigate the possibilities of different coloured plates, the edge emission of a large amount of coloured PMMA plates was measured (see Graph 13) using the set up described in Figure 22. These plates were purchased from Arkema[36], Evonik[37], Limacryl[45] and Perspex[35] and cut into 50x50mm plates. Although the surface areas of the different plates were similar, the thicknesses differed. As can be seen in Graph 13, almost the complete visible light spectrum is covered by the different edge emissions.

Several photocatalysts (MB, Eosin Y and $Ru(bpy)_3Cl_2$) were dissolved in acetonitrile and there absorption spectrum was measured by UV-VIS. Graph 14 shows the good overlap of the normalized absorption spectra with the normalized emission spectra of several coloured PMMA plates. This good overlap is very promising for further research on different coloured PMMA based LSC-PMs with different photocatalysts (see Chapter 7.2).

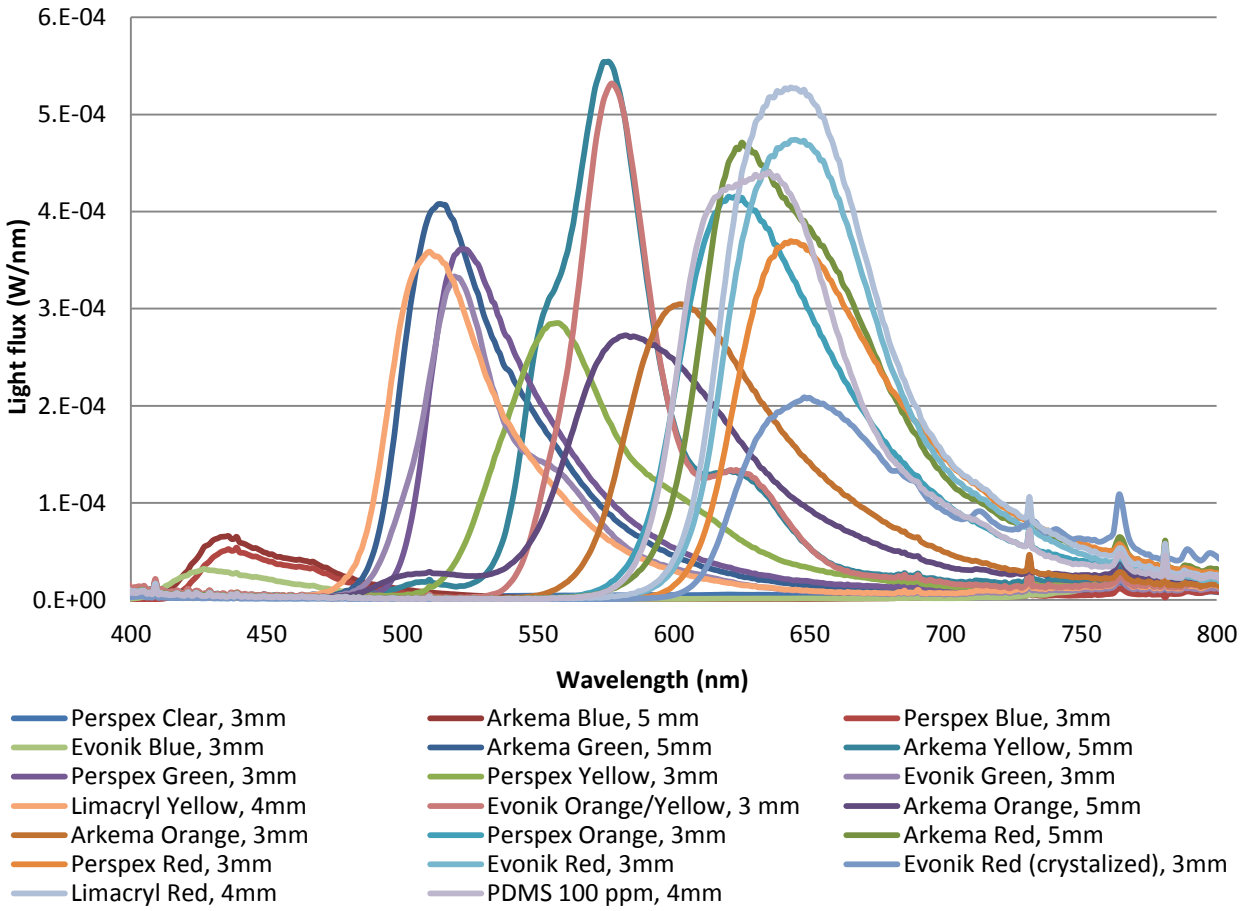

Graph 13: Edge emission measurements of different coloured 5x5cm plates with different thicknesses

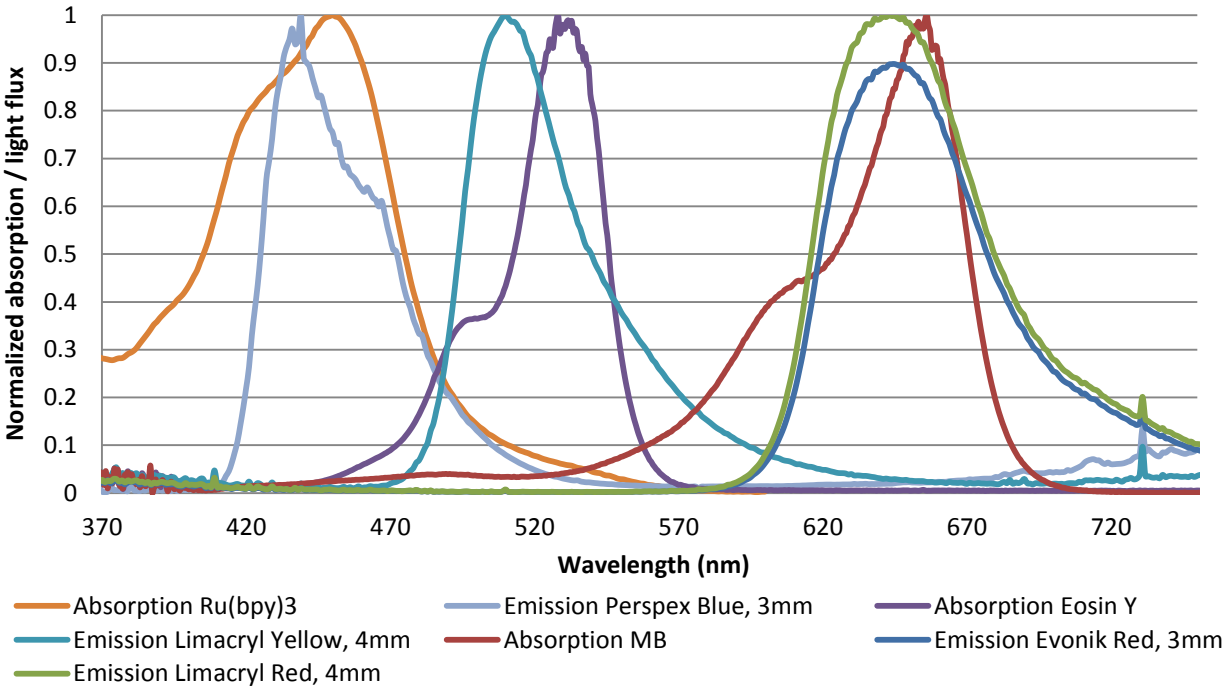

Graph 14: Normalized absorption measurements of different photocatalysts in MeCN and normalized edge emission measurements of different coloured 5x5 cm PMMA plates

6 Conclusion

In this research a successful attempt has been made to overcome the issues related to the previous PDMS based LSC-PMs. Several issues were solved by means of the addition of capillaries in the reactor design. A reliable manufacturing method was developed to add capillaries into the PDMS based LSC-PMs, with the use of completely 3D printed moulds (depth: 0.5 mm; radius: 95%; angle: 300°) and printed holders on HIPS plates. With the addition of the capillaries, the solvent compatibility of the reactor is enlarged to almost every solvent. The addition also prevented dye leaching from the matrix and reduced the change of leakage significantly.

Several capillary materials and dimensions were experimentally tested. It was found that the higher refractive index material, Tefzel, outperformed the PFA tubing. Therefore, it can be concluded that the refractive index of the polymer material is more significant than its transparency for this application. The dimensions of the tubing mostly influenced the light penetration depth through the reaction mixture. Therefore, the dimensions influenced both the throughput and the performances. Experiments showed that the performances of the capillary based LSC-PM were in the same range as the non-capillary reactors, proving that the addition of capillaries did not have a negative effect on the performances of the reactor. Lastly, a scale-up attempt of the PDMS based LSC-PM resulted in several issues.

Another matrix material, namely PMMA, has been investigated as well to overcome some issues related with the PDMS based LSC-PMs. A new, more straightforward, manufacturing method was developed for this material. Only drilling and pulling of the capillary was needed to create the PMMA based LSC-PMs. These capillary based PMMA reactors were known to be stable for a long period of time. Furthermore, different coloured reactors could be produced, widening the reaction scope significantly. Besides this, the reactors were much more rigid and significantly less expensive (20 times) compared to the PDMS based reactors.

Experiments showed a significant increase in the performances of the PMMA based LSC-PMs compared to the PDMS based reactors, due to the higher refractive index of PMMA. Different capillary materials did not have a significant influence of the performances of the PMMA based LSC-PM. After a scale-up attempt, stable 10x10cm^2, 20x20cm^2 and 30x30cm^2 reactors were produced. Hydroxylation reactions of arylboronic acids were performed inside these reactors, proving the production ability of these reactors. Stable slug flows were created inside the reactors, which was not possible in the previous design. The LSC-PMs significantly outperformed the original capillary designs without LSC by reducing the needed residence time with a factor of two. Lastly, the emission spectra of different coloured LSCs have been compared to the absorption spectra of different photocatalyst. This gave a promising expectation of widening the scope of the LSC-PMs to other photocatalysts.

To conclude, a broadly applicable red dye doped LSC-PM has been created, which solved all the issues related to the previous LSC-PM design. Furthermore, the reactor became much cheaper and easier to fabricate. Also the scale-up possibilities are experimentally shown. All these advantages have increased the industrial potential drastically. These promising results are a strong indication that, with the help of further research, the LSC-PM can be a successful device to make chemistry greener.

7 Recommendations for future work

Although a lot of promising results are obtained in this research, still several topics could be investigated in more depth. Several recommendations for future research will be discussed in more detail.

7.1 Checking residence times

Different sized PMMA based LSC-PMs were tested. It was expected that the larger reactors could possibly perform better, due to the relative decrease in reactor edge surface compared to the irradiated reactor surface. This could significantly decrease the amount of edge losses and therefore increase the reactor performances. However, as has been seen in chapter 5.6, no clear trend was visible in the different sized reactors. Furthermore, there is a large variation between the performances of the several sized LSC-PMs (see Graph 12).

It is known that flowrates can significantly differ from the summed gas and liquid flowrates due to consumption of the gas and due to the pressure drop over the reactor[46]. It can therefore be doubted whether the residence times in Graph 12, which are calculated from the summed gas and liquid flowrates, are reliable. Due to a different pressure drop over the different sized reactors, the error in the residence time could vary over the different sized reactors. It would therefore be sensible to check the residence times inside the different reactors. A tracer slug could be inserted and the residence time could be monitored for example by use of inline UV-VIS measurements. These corrections of the residence time could influence the results from Graph 12.

7.2 Different coloured reactors

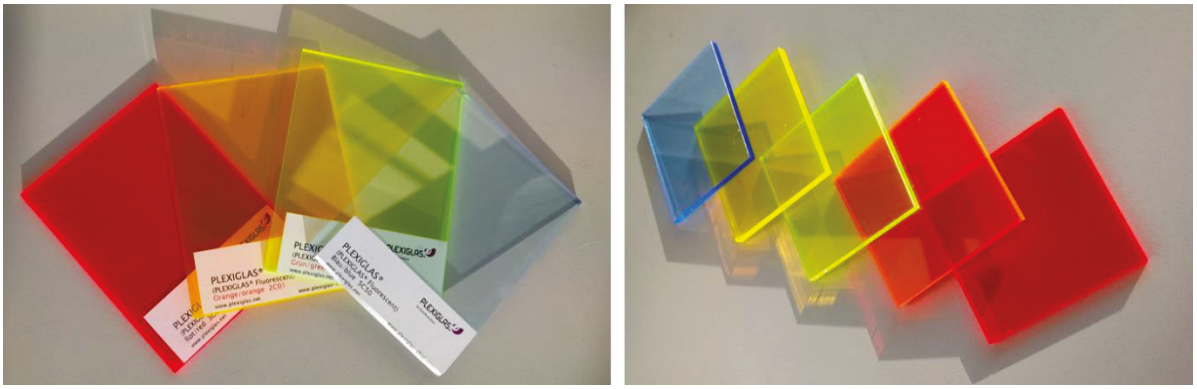

Figure 26: Fluorescent coloured PMMA plates purchased from Evonik[37] (left) and Perspex[35] (right)

It would be very interesting to test different photocatalyst within different coloured LSC-PMs. In this research it was already shown that the absorption of several photocatalyst had a perfect overlap with the emission of some fluorescent coloured PMMA plates (see chapter 5.7). It would be interesting to test several light-limited reactions inside the different coloured plates (Figure 26) and see the influence of the LSC-PMs. This could widen the scope of possible reactions inside a LSC-PM a lot. Furthermore, also a photocatalyst is known which provides different reaction potentials under irradiation of different coloured light[47]. Therefore, follow-up reactions can be performed by sequential irradiation of two different coloured light sources. It would be interesting to see whether these reactions can also be performed under sunlight while flowing through two different coloured LSC-PMs. Ideally these LSC-PMs could be placed on top of each other, since they both absorb different parts of the solar spectrum.

7.3 New production method for scaled up devices

In this research a quite straight forward scaling up method for PMMA based LSC-PMs has been proposed. Although relative large sized reactors were obtained, this method still has some drawbacks. First of all, pulling the capillary through the plates is a very time intensive job. Furthermore, a lot of tension is created on the tubing when pulling a capillary through the PMMA plates. This tension could deform the capillary and could result in easy breakage of the tubing. Certainly when the separate 5cm plates need to be brought together, a lot of tension is created. Lastly, the separate 5cm PMMA plates result in a quite flexible design and make the largely sized reactors less rigid. These challenges make scaling up to larger dimensions (e.g. $1m^2$) difficult and decrease therefore the potential for industrial applications.

Further investigation on scale up methods could overcome these issues. Two possible production methods are proposed (see Figure 27). In both designs half circles are drilled/scratched in several PMMA plates. Capillaries can be added between the half circled PMMA plates. These plates can be fitted together by use of clamps. In the first production method (Figure 27A), the clamp is horizontally orientated on several long plates. With this method the capillary can reach till the top and bottom of the PMMA plate. This could minimize the losses due to a minimization of guided light passing by the capillary inside the PMMA plate (see Figure 28). In the second production method (Figure 27B), the clamps are orientated vertically to tighten two PMMA plates on top of each other. With this method it would be possible to keep the capillary within the reactor by making the bending inside the plates instead of outside. My personal preference would be this second production method, since the capillary could stay inside the reactor and no huge clamps are needed for large reactors. Furthermore, this reactor design could create a less fragile reactor. Of course the effect of the interface between the two PMMA plates on the performances of the reactor should be tested.

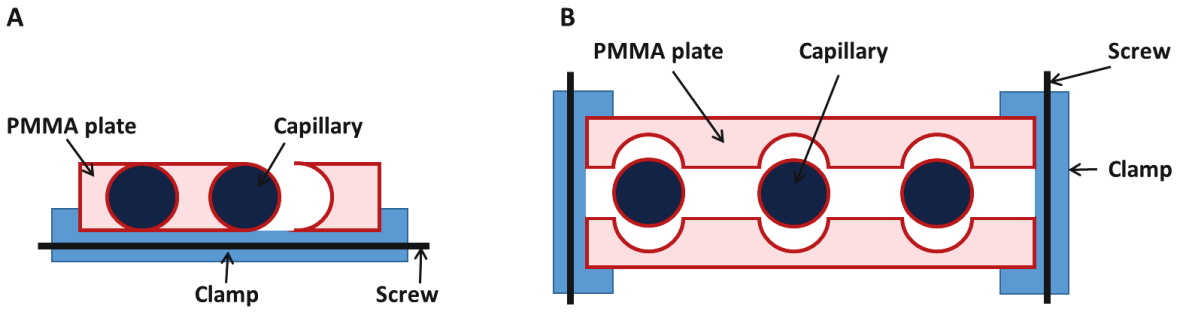

Figure 27: Two possible scale-up production methods for the PMMA based LSC-PMs

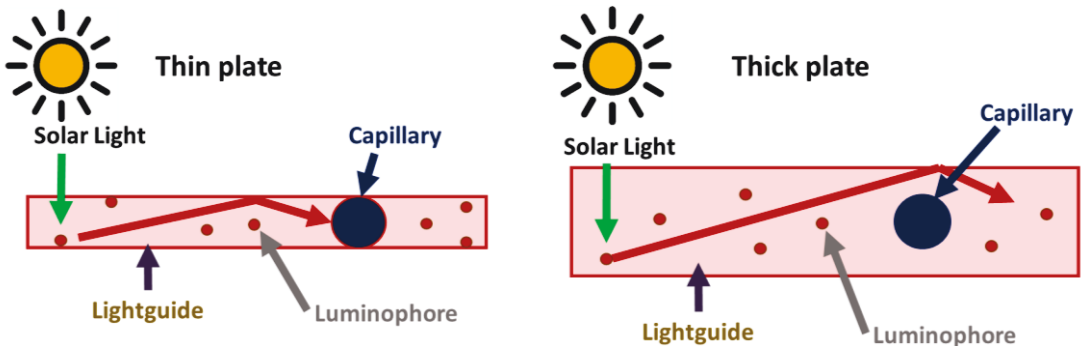

Figure 28: Comparison of light guiding through thin (left) and thick (right) LSC plates. The change of guided light passing by the reaction channel is larger within thick plates compared to thinner LSC plates.

7.4 Automated light response system

Light intensities from sunlight can vary a lot over time due to clouds and day-night cycles. To maintain full conversion inside the LSC-PM, different residence times would be needed at different light intensities. It would be interesting to create a system which is able to check the light intensities with help of a light sensor and controls the flow rates automatically. This would create the possibility to automatically run photochemical reactions outdoor in a LSC-PM. Before applying a light response system, the performances of the LSC-PM should firstly be tested under outdoor conditions.

8 Acknowledgments

I would gladly like to thank my daily supervisor Dario Cambié, my supervisor Timothy Noël and my graduation professor Volker Hessel for the opportunity to conduct my master thesis within the SCR-SFP group. I had a great time within the group and enjoyed every moment of working on this project. I learned a lot about chemical engineering and chemistry, but also about the academic world.

Firstly, I would like to thank Dario, with whom I worked so closely together during the last 9 months. I really appreciate all your help and the effort you put into the project. Your open, enthusiastic and helpful attitude was always a warm welcome when coming to the university.

Furthermore, I would like to thank Timothy for his trust in my ideas and for his constant believe in the project and Michael Debije for his enthusiasm, helpfulness and his tremendous amount of knowledge about LSCs. Passing by your offices was always a pleasant moment. I would also like to acknowledge Erik van Herk for his work on producing the PMMA based LSC-PMs.

Furthermore, I would like to thank the whole group for all the enjoyable time on the lab, during the lunch and during the activities. I would like to thank: Fang for the good collaboration on the LSC-PM project. Koen for all the long conversations, pub-quizzes, cycling tours and stupid Dumpert videos. Hannes for his ride back from Rotterdam in the middle of the night. Gabriële for all his good (and loud) stories and always positive attitude. Of course I would also like to thank Cecilia and Xiao-Jing for creating such a great atmosphere within the group. Furthermore, I would like to thank all the students with who I worked side by side during my project. In specific, Jeroen, Koen and Menno, with whom I started together 9 months ago. I have had a great time with you.

Lastly, I would like to thank my family, my friends and my girlfriend Nadia for all their support during my master thesis.

Thanks to all of you, I had a great time during my graduation project.

9 Bibliography

(1) Cambié, D.; Zhao, F.; Hessel, V.; Debije, M. G.; Noël, T. A Leaf-Inspired Luminescent Solar Concentrator for Energy-Efficient Continuous-Flow Photochemistry. *Angew. Chemie Int. Ed.* **2017**, *56* (4), 1050–1054.

(2) Obama, B. The Irreversible Momentum of Clean Energy. *Science (80-.).* **2017**, *6284* (January).

(3) Vaccaro, L.; Lanari, D.; Marrocchi, A.; Strappaveccia, G. Flow Approaches towards Sustainability. *Green Chem.* **2014**, *16* (8), 3680.

(4) Cambié, D.; Bottecchia, C.; Straathof, N. J. W.; Hessel, V.; Noël, T. Applications of Continuous-Flow Photochemistry in Organic Synthesis, Material Science, and Water Treatment. *Chem. Rev.* **2016**, acs.chemrev.5b00707.

(5) Su, Y.; Straathof, N. J. W.; Hessel, V.; Noël, T. Photochemical Transformations Accelerated in Continuous-Flow Reactors: Basic Concepts and Applications. *Chem. - A Eur. J.* **2014**, *20* (34), 10562–10589.

(6) Ciamician, G. The Photochemistry of the Future. *Science (80-.).* **1912**, *36* (926), 385–394.

(7) Schultz, D. M.; Yoon, T. P. Solar Synthesis: Prospects in Visible Light Photocatalysis. *Science (80-.).* **2014**, *343* (6174), 1239176.

(8) Scholes, G. D.; Fleming, G. R.; Olaya-Castro, A.; van Grondelle, R. Lessons from Nature about Solar Light Harvesting. TL - 3. *Nat. Chem.* **2011**, *3 VN-re* (10), 763–774.

(9) Hoffmann, N. Photochemical Reactions of Aromatic Compounds and the Concept of the Photon as a Traceless Reagent. *Photochem. Photobiol. Sci.* **2012**, *11* (11), 1613.

(10) Romero, N. A.; Nicewicz, D. A. Organic Photoredox Catalysis. **2016**.

(11) Prier, C. K.; Rankic, D. A.; MacMillan, D. W. C. Visible Light Photoredox Catalysis with Transition Metal Complexes: Applications in Organic Synthesis. *Chem. Rev.* **2013**, *113* (7), 5322–5363.

(12) Hessel, V.; Angeli, P.; Gavriilidis, A.; Löwe, H. Gas-Liquid and Gas-Liquid-Solid Microstructured Reactors: Contacting Principles and Applications. *Ind. Eng. Chem. Res.* **2005**, *44* (25), 9750–9769.

(13) Fujiya, A.; Tanaka, M.; Yamaguchi, E.; Tada, N.; Itoh, A. Sequential Photo-Oxidative [3 + 2] Cycloaddition/Oxidative Aromatization Reactions for the Synthesis of Pyrrolo[2,1-A]isoquinolines Using Molecular Oxygen as the Terminal Oxidant. *J. Org. Chem.* **2016**, *81* (16), 7262–7270.

(14) Malato, S.; Fernandez-Ibanez, P.; Maldonado, M. I.; Blanco, J.; Gernjak, W. Decontamination and Disinfection of Water by Solar Photocatalysis: Recent Overview and Trends. *Catal. Today* **2009**, *147* (1), 1–59.

(15) Schiel, C.; Oelgemöller, M.; Ortner, J.; Mattay, J. Green Photochemistry: The Solar-Chemical "Photo–Friedel–Crafts Acylation"of Quinones. *Green Chem.* **2001**, 224–228.

(16) Dondi, D.; Protti, S.; Albini, A.; Carpio, S. M.; Fagnoni, M. Synthesis of γ-Lactols, γ-Lactones and 1,4-Monoprotected Succinaldehydes under Moderately Concentrated Sunlight. *Green Chem.* **2009**, *11* (10), 1653.

(17) Oelgemöller, M. Solar Photochemical Synthesis: From the Beginnings of Organic Photochemistry to the Solar Manufacturing of Commodity Chemicals. *Chem. Rev.* **2016**, *116* (17), 9664–9682.

(18) Nauth, A. M.; Lipp, A.; Lipp, B.; Opatz, T. Sunflow: Sunlight Drives Fast and Green Photochemical Flow Reactions in Simple Microcapillary Reactors - Application to Photoredox and H-Atom-Transfer Chemistry. *European J. Org. Chem.* **2016**, 1–6.

(19) Mirkovic, T.; Ostroumov, E. E.; Anna, J. M.; van Grondelle, R.; Govindjee; Scholes, G. D. Light Absorption and Energy Transfer in the Antenna Complexes of Photosynthetic Organisms. *Chem. Rev.* **2016**, acs.chemrev.6b00002.

(20) Overmann, J.; Cypionka, H.; Pfennig, N. An Extremely Low-Light Adapted Phototrophic Sulfur Bacterium from the Black Sea. *Limnol. Oceanogr.* **1992**, *37* (1), 150–155.

(21) Debije, M. G.; Verbunt, P. P. C. Thirty Years of Luminescent Solar Concentrator Research: Solar Energy for the Built Environment. *Adv. Energy Mater.* **2012**, *2* (1), 12–35.

(22) van Sark, W. G. J. H. M. Luminescent Solar Concentrators - A Low Cost Photovoltaics Alternative. *Renew. Energy* **2013**, *49*, 207–210.

(23) Slooff, L. H.; Bende, E. E.; Burgers, A. R.; Budel, T.; Pravettoni, M.; Kenny, R. P.; Dunlop, E. D.; Büchtemann, A. A Luminescent Solar Concentrator with 7.1% Power Conversion Efficiency. *Phys. Status Solidi - Rapid Res. Lett.* **2008**, *2* (6), 257–259.

(24) Lee, J. N.; Park, C.; Whitesides, G. M. Solvent Compatibility of Poly(dimethylsiloxane)-Based Microfluidic Devices. *Anal. Chem.* **2003**, *75* (23), 6544–6554.

(25) Halldorsson, S.; Lucumi, E.; Gómez-Sjöberg, R.; Fleming, R. M. T. Advantages and Challenges of Microfluidic Cell Culture in Polydimethylsiloxane Devices. *Biosens. Bioelectron.* **2015**, *63*, 218–231.

(26) Gutierrez, A. C.; Jamison, T. F. Scalable and Robust Synthesis of $CpRu(MeCN)_3PF_6$ via Continuous Flow Photochemistry. *J. Flow Chem.* **2011**, *1* (1), 24–27.

(27) Resin, M. DuPont Tefzel 280.

(28) Melker, A.; Fors, B. P.; Hawker, C. J.; Poelma, J. E. Continuous Flow Synthesis of Poly(methyl Methacrylate) via a Light-Mediated Controlled Radical Polymerization. *J. Polym. Sci. Part A Polym. Chem.* **2015**, *53* (23), 2693–2698.

(29) Dow Corning. *Electronics Sylgard ® 184 Silicone Elastomer*; 2013.

(30) Pitre, S. P.; McTiernan, C. D.; Vine, W.; DiPucchio, R.; Grenier, M.; Scaiano, J. C. Visible-Light Actinometry and Intermittent Illumination as Convenient Tools to Study Ru(bpy)3Cl2 Mediated Photoredox Transformations. *Sci. Rep.* **2015**, *5* (October), 16397.

(31) Bergmann, K.; O'Konski, C. T. A Spectroscopic Study of Methylene Blue Monomer, Dimer, and Complexes With Montmorillonite. *J. Phys. Chem.* **1963**, *67* (10), 2169–2177.

(32) *Polymer Data Handbook*; Oxford University Press, 1999.

(33) Mapel, J. Luminescent Solar Concentrators. **1982**, *29* (4), 323–329.

(34) Sark, W. G. J. H. M. Van; Barnham, K. W. J.; Slooff, L. H.; Chatten, A. J.; Büchtemann, A.; Meyer, A.; Mccormack, S. J.; Koole, R.; Farrell, D. J.; Bose, R.; et al. Luminescent Solar

Concentrators – A Review of Recent Results. **2008**, *16* (26), 21773–21792.

(35) Perspex http://www.perspex.co.uk/ (accessed Apr 10, 2017).

(36) Arkema http://www.arkema.com/en/ (accessed Apr 10, 2017).

(37) Evonik https://www.plexiglas-shop.com (accessed Apr 10, 2017).

(38) Wiley. *Processing and Finishing of Polymeric Materials*, 2nd ed.; 2012.

(39) Vishwanathan, B.; Reinders, A. H. M. E.; de Boer, D. K. G.; Desmet, L.; Ras, A. J. M.; Zahn, F. H.; Debije, M. G. A Comparison of Performance of Flat and Bent Photovoltaic Luminescent Solar Concentrators. *Sol. Energy* **2015**, *112*, 120–127.

(40) Chen, M.; Johnson, J. A. Improving Photo-Controlled Living Radical Polymerization from Trithiocarbonates through the Use of Continuous-Flow Techniques. *Chem. Commun.* **2015**, *51* (31), 6742–6745.

(41) Pitre, S. P.; McTiernan, C. D.; Ismaili, H.; Scaiano, J. C. Mechanistic Insights and Kinetic Analysis for the Oxidative Hydroxylation of Arylboronic Acids by Visible Light Photoredox Catalysis: A Metal-Free Alternative. *J. Am. Chem. Soc.* **2013**, *135* (36), 13286–13289.

(42) Cocquet, G.; Ferroud, C.; Guy, A. A Mild and Efficient Procedure for Ring-Opening Reactions of Piperidine and Pyrrolidine Derivatives by Single Electron Transfer Photooxidation. *Tetrahedron* **2000**, *56* (19), 2975–2984.

(43) Pitre, S. P.; McTiernan, C. D.; Ismaili, H.; Scaiano, J. C. Metal-Free Photocatalytic Radical Trifluoromethylation Utilizing Methylene Blue and Visible Light Irradiation. *ACS Catal.* **2014**, *4* (8), 2530–2535.

(44) Zou, Y.-Q.; Chen, J.-R.; Liu, X.-P.; Lu, L.-Q.; Davis, R. L.; Jørgensen, K. A.; Xiao, W.-J. Highly Efficient Aerobic Oxidative Hydroxylation of Arylboronic Acids: Photoredox Catalysis Using Visible Light. *Angew. Chem. Int. Ed. Engl.* **2012**, *51*, 784–788.

(45) Limacryl http://www.limacryl.be (accessed Apr 18, 2017).

(46) Su, Y.; Hessel, V.; Noël, T. A Compact Photomicroreactor Design for Kinetic Studies of Gas-Liquid Photocatalytic Transformations. *AIChE J.* **2015**, *61* (7), 2215–2227.

(47) Ghosh, I.; König, B. Chromoselective Photocatalysis: Controlled Bond Activation through Light-Color Regulation of Redox Potentials. *Angew. Chemie - Int. Ed.* **2016**, *55* (27), 7676–7679.

(48) Reference Solar Spacrtal Irradiance: Air Mass 1.5 http://rredc.nrel.gov/solar/spectra/am1.5/ (accessed May 4, 2017).

(49) Debije, M. G.; Menelaou, C.; Herz, L. M.; Schenning, A. P. H. J. Combining Positive and Negative Dichroic Fluorophores for Advanced Light Management in Luminescent Solar Concentrators. *Adv. Opt. Mater.* **2014**, *2* (7), 687–693.

10 Nomenclature

Abbreviation	Meaning
ACN	Acetonitrile
DPA	1,9-diphenylanthracene
Halar	Ethylene Chlorotrifluoroethylene
ID	Inner diameter
LR305	Lumogen Red 305 (purchased from BASF)
LSC	Luminescent Solar Concentrator
LSC-PM	Luminescent Solar Concentrator Photo Microreactor
MB	Methylene Blue
OD	Outer diameter
PDMS	Polydimethylsiloxane
PFA	Perfluoroalkoxy
PMMA	Polymethyl methacrylate
RI	Refractive Index
Tefzel	Ethylene tetrafluoroethylene

Symbol	Meaning	Unit
A	Absorbance	-
C	Molar concentration	mol/L
c	Speed of light	m/s
d	Path length of the beam travelling through a medium	cm
h	Planck constant	J s
I	Intensity	W/m^2
n	Refractive index	-
N_A	Avogadro number	mol^{-1}
ε	Extinction coefficient	$M^{-1}cm^{-1}$
Θ	Angle	°
λ	Wavelength	m
φ_{light}	Light flux	W/nm
φ_{ph}	Photon flux	Photons $(nm\ s)^{-1}$

Appendix I

Toluene was flushed through a red PDMS based LSC-PM without capillary. Graph 15 shows the UV-VIS spectra of this flushed toluene and of a solution of the fluorescent red dye (LR305) in toluene. It can be seen that both spectra have a similar shape, proving that LR305 is leaching from the PDMS reactor into the reaction mixture.

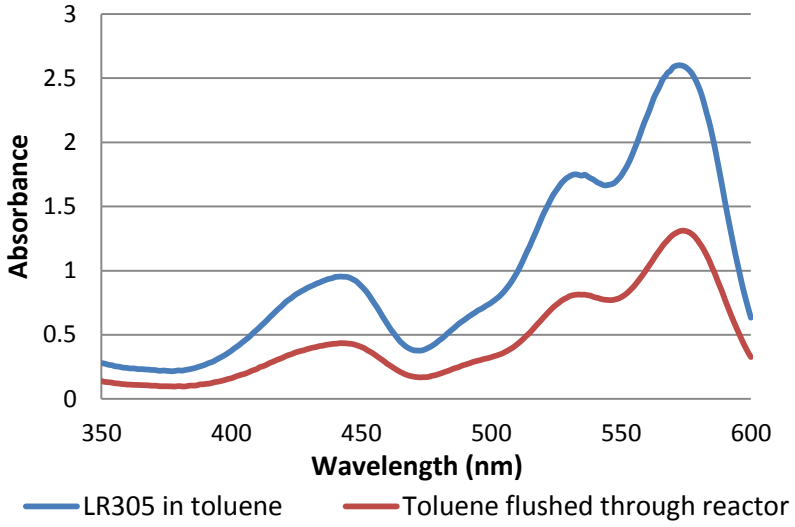

Graph 15: UV-VIS spectrum of LR305 in toluene (blue) and toluene leaving the reactor after leaching of the dye (red)

Appendix II

Spectra of used light sources

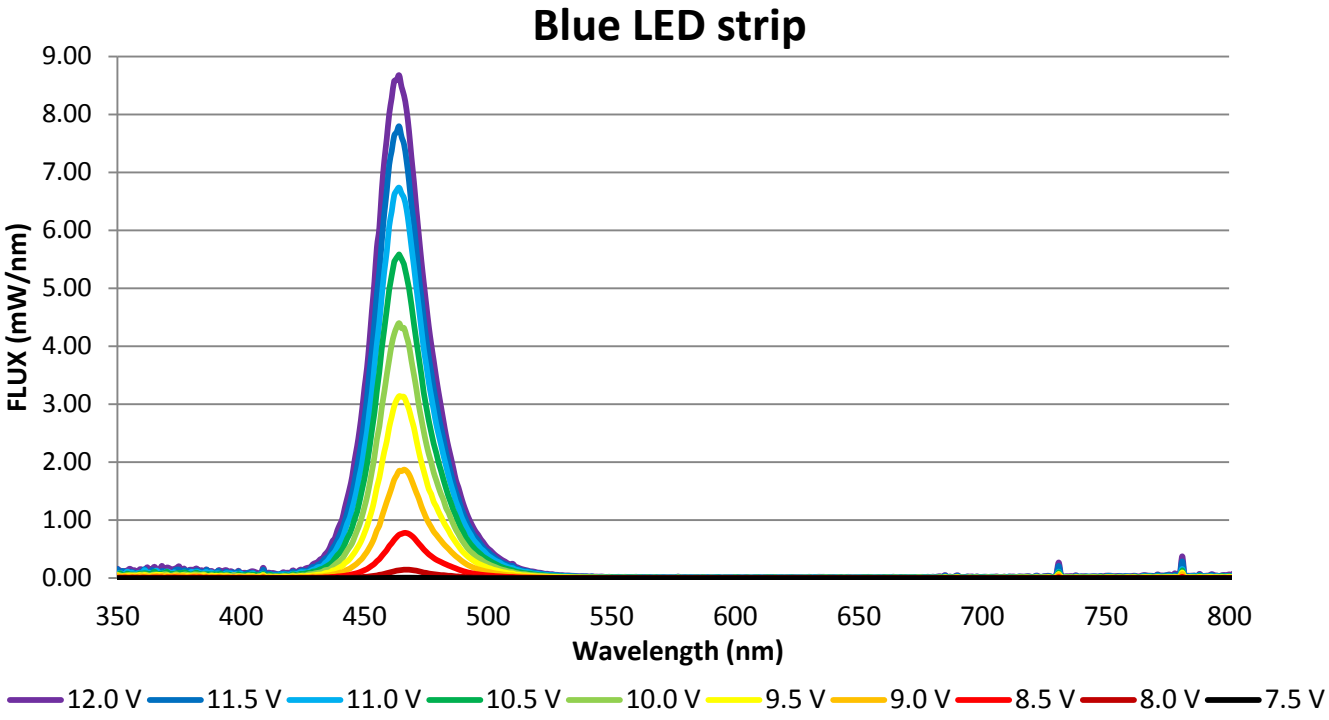

Graph 16: Emission spectrum of the used blue LED strip at different voltages

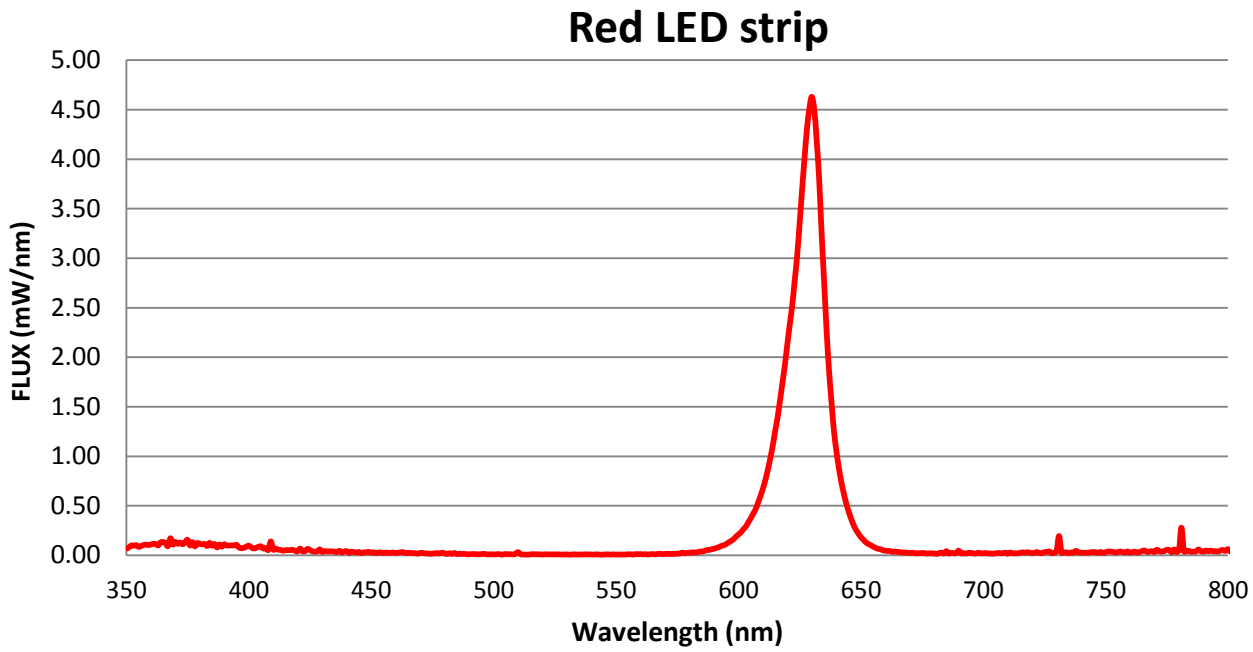

Graph 17: Emission spectrum of the used red LED strip

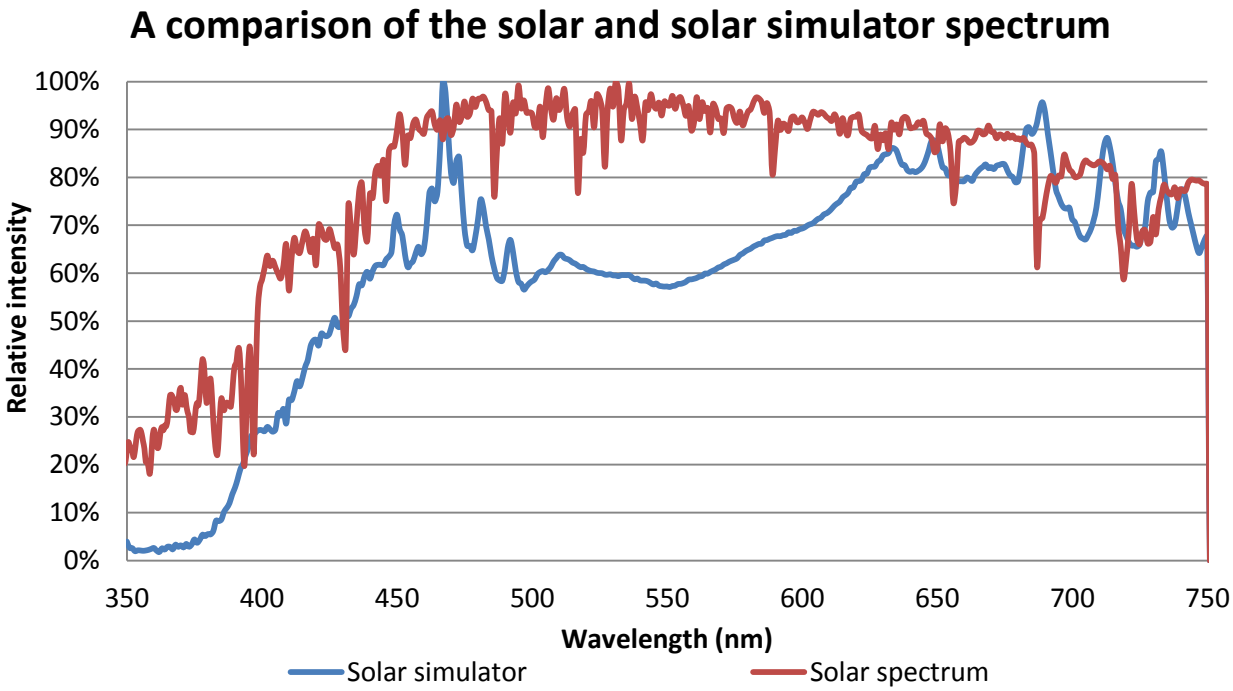

Graph 18: Comparison of the emission spectra of the solar light and of the solar simulator used for edge emission measurements (LS0110-100, L.O.T.). (Solar spectrum is obtained from [48])

Appendix III

Both a custom made 100 ppm LR305 doped 4 mm thick PMMA plate (Limacryl) and a fluorescent red 3 mm thick plate (Evonik) were purchased. The used dye and dye loading of the commercially purchased Evonik plate were unknown. Therefore UV-VIS measurements of both plates were taken (see Graph 19). Firstly, these two similar spectra prove that the Evonik plates also contained the LR305 dye. Furthermore, the dye loading of the Evonik plate could be calculated by use of the two spectra. The two peak areas from 457-655 nm were measured (Limacryl: 153.2; Evonik: 129.4). The dye loading of the Evonik plate could be calculated by use of these peak areas, the different thicknesses of the plates and the dye loading of the Limacryl plate (100 ppm), as follows:

$$\text{Loading Evonik} = \frac{\frac{\text{area Evonik}}{\text{thickness Evonik}}}{\frac{\text{area Limacryl}}{\text{thickness limacryl}}} \bullet \text{loading Limacryl} = \frac{\frac{129.4}{3}}{\frac{152.2}{4}} \bullet 100 = 113 \text{ ppm}$$

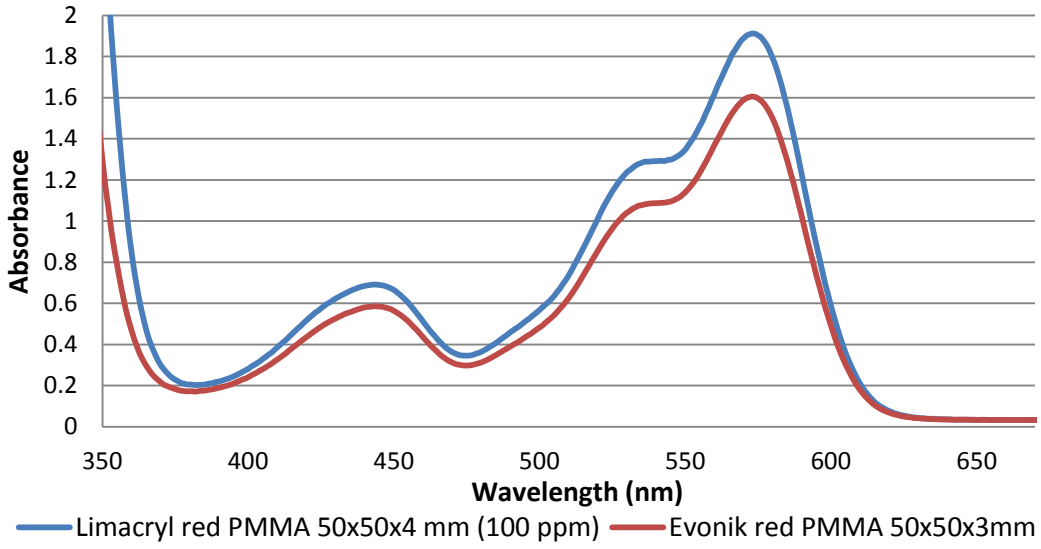

Graph 19: UV-VIS spectrum of two fluorescent red PMMA plates

Appendix IV

Chemical structures fluorescent dyes

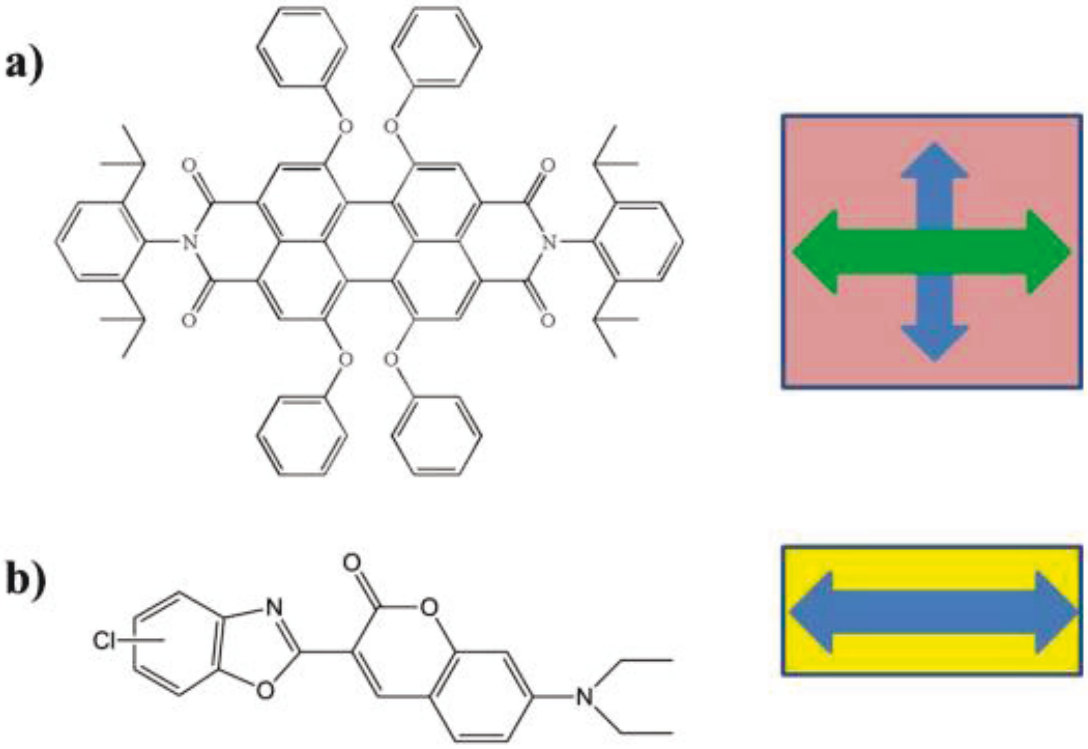

Figure 29: Chemical structure of Lumogen F red 305 purchased from BASF (A) and of coumarin yellow (DFSB-K160) (B). The boxes to the right of the structures show the main absorption dipole directions (arrow). The arrow colour corresponds to the absorbed wavelength regions; the colour of the surrounding box corresponds to the visible colour of the dye. (Picture obtained from [49])

Chemical structures polymeric matrix materials

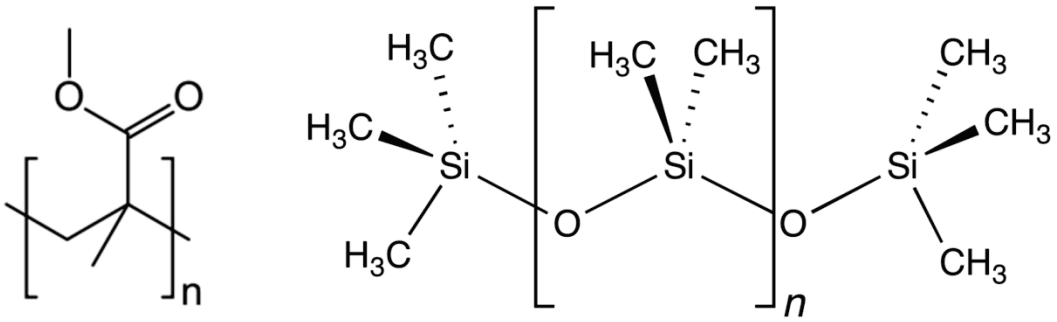

Figure 30: Chemical structure of the repeating unit of PMMA (left) and PDMS (right).

Chemical structures photocatalysts

Methylene Blue

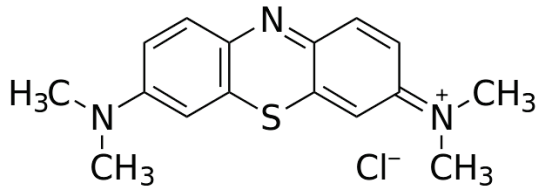

Eosin Y

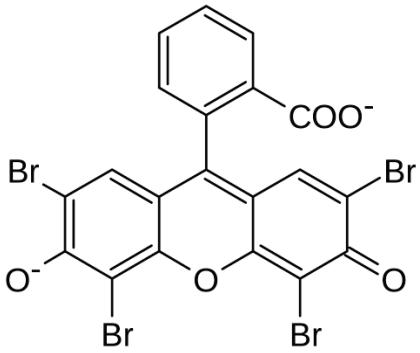

$Ru(bpy)_3Cl_2$